Quaternary Science Reviews 103 (2014) 116–133

Contents lists available at ScienceDirect

Quaternary Science Reviews

journal homepage: www.elsevier.com/locate/quascirev

Temporal and spatial structure of multi-millennial temperature changes at high latitudes during the Last Interglacial

Emilie Capron [a, *], Aline Govin [b], Emma J. Stone [c], Valérie Masson-Delmotte [d], Stefan Mulitza [b], Bette Otto-Bliesner [e], Tine L. Rasmussen [f], Louise C. Sime [a], Claire Waelbroeck [d], Eric W. Wolff [g]

[a] British Antarctic Survey, High Cross, Madingley Road, CB3 0ET Cambridge, UK
[b] MARUM/Center for Marine Environmental Sciences, University of Bremen, Leobener Strasse, 28359 Bremen, Germany
[c] BRIDGE, School of Geographical Sciences, University of Bristol, Bristol BS8 1SS, UK
[d] Institut Pierre-Simon Laplace/Laboratoire des Sciences du Climat et de l'Environnement, UMR 8212, CEA-CNRS-UVSQ, 91191 Gif-sur-Yvette, France
[e] Climate and Global Dynamics Division, National Center for Atmospheric Research (NCAR), Boulder, CO 80305, USA
[f] CAGE-Centre for Arctic Gas Hydrate, Environment and Climate, UiT, the Arctic University of Norway, Tromsø, Norway
[g] Godwin Laboratory for Palaeoclimate Research, Department of Earth Sciences, University of Cambridge, CB2 3EQ Cambridge, UK

ARTICLE INFO

Article history:
Received 31 March 2014
Received in revised form
20 August 2014
Accepted 22 August 2014
Available online 3 October 2014

Keywords:
Last Interglacial period
Marine sediment cores
Ice cores
Data synthesis
Climate model simulations

ABSTRACT

The Last Interglacial (LIG, 129–116 thousand of years BP, ka) represents a test bed for climate model feedbacks in warmer-than-present high latitude regions. However, mainly because aligning different palaeoclimatic archives and from different parts of the world is not trivial, a spatio-temporal picture of LIG temperature changes is difficult to obtain.

Here, we have selected 47 polar ice core and sub-polar marine sediment records and developed a strategy to align them onto the recent AICC2012 ice core chronology. We provide the first compilation of high-latitude temperature changes across the LIG associated with a coherent temporal framework built between ice core and marine sediment records. Our new data synthesis highlights non-synchronous maximum temperature changes between the two hemispheres with the Southern Ocean and Antarctica records showing an early warming compared to North Atlantic records. We also observe warmer than present-day conditions that occur for a longer time period in southern high latitudes than in northern high latitudes. Finally, the amplitude of temperature changes at high northern latitudes is larger compared to high southern latitude temperature changes recorded at the onset and the demise of the LIG.

We have also compiled four data-based time slices with temperature anomalies (compared to present-day conditions) at 115 ka, 120 ka, 125 ka and 130 ka and quantitatively estimated temperature uncertainties that include relative dating errors. This provides an improved benchmark for performing more robust model-data comparison. The surface temperature simulated by two General Circulation Models (CCSM3 and HadCM3) for 130 ka and 125 ka is compared to the corresponding time slice data synthesis. This comparison shows that the models predict warmer than present conditions earlier than documented in the North Atlantic, while neither model is able to produce the reconstructed early Southern Ocean and Antarctic warming. Our results highlight the importance of producing a sequence of time slices rather than one single time slice averaging the LIG climate conditions.

1. Introduction

Due to numerous positive feedbacks, polar regions act as amplifiers of climate change (e.g. CAPE Last Interglacial Project Members, 2006; Masson-Delmotte et al., 2013; Nikolova et al., 2013). During the last decade, the Arctic has experienced the strongest warming trend observed at the Earth's surface, and further climate change is expected to produce large environmental changes in the near future including Arctic glaciers and Greenland ice sheet contributions to projected sea level rise (Church et al., 2013). By contrast, recent sea ice and temperature trends in and around Antarctica appear more complex, and this area is expected

* Corresponding author. Tel.: +44 1223 221 368; fax: +44 1223 362 616.
E-mail address: ecap@bas.ac.uk (E. Capron).

http://dx.doi.org/10.1016/j.quascirev.2014.08.018

to respond on longer time scales to increased greenhouse gas emissions, with large uncertainties on associated sea level risks. The ability of climate models to correctly capture feedbacks involved in polar amplification remains uncertain and past climatic changes provide benchmarks against which the realism of climate models can be assessed (Braconnot et al., 2012; Schmidt et al., 2014). In particular, studying past warm periods such as recent interglacial periods, provide unique insights to assess polar amplification feedbacks in a range of temperature changes comparable to projected future changes (e.g. Otto-Bliesner et al., 2013).

The Last Interglacial period (hereafter LIG; 129–116 thousand of years BP, hereafter ka) is of particular interest since large parts of the globe were characterised by a warmer-than-present day climate (e.g. CAPE Last Interglacial Project Members, 2006; Turney and Jones, 2010). While orbital insolation was distinctly different to present-day (Laskar et al., 2004), atmospheric CO_2 concentration levels were close to pre-industrial values (Lüthi et al., 2008). The LIG is not an analogue for future climate change because orbital forcing is fundamentally different from anthropogenic forcing, and because the geographical pattern of LIG temperature changes strongly differ from those expected in the future (Masson-Delmotte et al., 2011a). Nonetheless, it offers an opportunity to assess the effect of warmer-than-present-day polar climate on climate-sensitive parts of the Earth system, most notably polar ice sheets and sea level. Previous work suggests that global sea level was 5.5–9 m higher than today (e.g. Kopp et al., 2009; Thompson et al., 2011). Combined with earlier evidence for LIG ice at the bottom of the Greenland ice sheet (e.g. GRIP members, 1993), the NEEM ice core data demonstrate the resilience of the central Greenland ice sheet to LIG local warming (NEEM community members, 2013). Ice sheet simulations compatible with NEEM elevation estimates suggest that the Greenland ice sheet contribution to the sea level rise should be in the range of 1.4–4.3 m (Robinson et al., 2011; Born and Nisancioglu, 2012; Masson-Delmotte et al., 2013; Quiquet et al., 2013; Stone et al., 2013). However, different input climates arising from climate simulations have been used as inputs for these ice sheet simulations. Also, the study of the LIG benefits from numerous snapshot and transient climatic simulations with state of the art General Circulation Models (GCMs; e.g. Bakker et al., 2013; Lunt et al., 2013; Nikolova et al., 2013; Otto-Bliesner et al., 2013; Langebroek and Nisancioglu, 2014; Paleoclimate Modelling Intercomparison Project, http://pmip3.lsce.ipsl.fr/). Altogether, this further motivates the evaluation of these GCMs against LIG climate reconstructions. In particular, data syntheses are required to document the magnitude and spatio-temporal structure of LIG temperature changes.

Several climatic data compilation initiatives have been conducted for the LIG (CLIMAP, 1984; Kaspar et al., 2005; CAPE Last Interglacial Project Members, 2006; Clark and Huybers, 2009; Turney and Jones, 2010; McKay et al., 2011). Turney and Jones (2010) averaged temperature estimates across the benthic foraminifera $\delta^{18}O$ and ice $\delta^{18}O$ plateau in marine and ice core records respectively, and across the period of maximum warmth in terrestrial sequences. They deduced a global annual LIG "maximum" warming above pre-industrial of about 2 °C and they identified earlier warming in Antarctica. McKay et al. (2011) used an alternative temperature-averaging method and calculated the mean sea surface temperature (SST) over a 5 ka period centred on the warmest temperature observed between 135 ka and 118 ka in marine records. They estimated a global annual mean SST warming of $+0.7 \pm 0.6$ °C relative to the late Holocene.

Otto-Bliesner et al. (2013) used these existing LIG temperature compilations to benchmark snapshot simulations performed at 125 and 130 ka with the CCSM3 GCM. However, both time slices are compared to a single data synthesis built assuming explicitly synchronous peak warmth. Recently, Bakker et al. (2014) proposed a comparison of temperature rates of change inferred from transient simulations as well as sea surface temperature (SST) from alkenone data and polar temperature syntheses, albeit without common chronologies. Both studies stress uncertainties associated with chronologies and temperature-averaging procedures. A temporal description of the LIG climate rather than an asynchronous compilation of LIG temperature optima could allow a detailed evaluation of these model simulations.

Indeed, current temporal representations inferred from marine sediment and ice core records remain limited so far by the lack of a common robust age scale over the LIG. Existing LIG syntheses are currently based on records taken on their original timescale, introducing absolute dating uncertainties that can reach several thousand years (e.g. Waelbroeck et al., 2008; Bazin et al., 2013; Veres et al., 2013). However, there is evidence that surface temperature peaks are not globally coincident. In particular, there is a significant delay in the establishment of peak interglacial conditions in the North Atlantic and Nordic Seas as compared to the Southern Ocean (Cortijo et al., 1999; Bauch and Erlenkeuser, 2008; Bauch et al., 2011; Van Nieuwenhove et al., 2011; Govin et al., 2012). Also, an early Antarctic warming has been reported (Masson-Delmotte et al., 2010). Thus, a compilation with a dynamic representation of the sequence of climatic events (several time slices) taking into account potential asynchronous temperature changes between the two hemispheres during the LIG is necessary. This requires synchronising palaeoclimatic records from different archives (e.g. ice cores and marine sediments).

The objectives of this study are twofold. First we document the magnitude and spatio-temporal structure of LIG temperature changes in the high latitudes of the two hemispheres. For that purpose, we describe a new data synthesis of air and sea surface temperature changes across the LIG in polar and sub polar regions associated with a coherent temporal framework between ice core and marine sediment records. Second, based on this new high latitude data compilation, we produce four data-based surface temperature anomaly time slices at 115 ka, 120 ka, 125 ka and 130 ka for which we propagate relative dating uncertainties and reconstructed temperature errors into the final temperature anomaly estimates. Using snapshot simulations performed for the 125 ka and 130 ka climatic conditions by the CCSM3 and HadCM3 models, we illustrate how these new time slices enable more robust model-data comparison to be performed in order to test state-of-the-art GCMs also used to perform future climate projections.

2. Material and methods

2.1. Palaeoclimatic data selection

We selected sites presenting a mean time-resolution of temperature reconstruction better than 2 ka and sufficient additional information (e.g. benthic and/or planktic $\delta^{18}O$ records, ash layers) to help integrate them with confidence into the common temporal framework. We selected five records of surface air temperature deduced from water stable isotopes measured along polar ice cores and 42 SST records from marine sediment cores located above 40°N and 40°S of latitude (Fig. 1). We obtained data through the PANGAEA database, from individual papers provided by principal investigators or extracted from published figures through digital image processing. Details for each selected record are given in Table A1.

- *Ice core records*:

We include local surface air temperature reconstructions for the East Antarctic EPICA Dome C (EDC), EPICA Dronning Maud Land

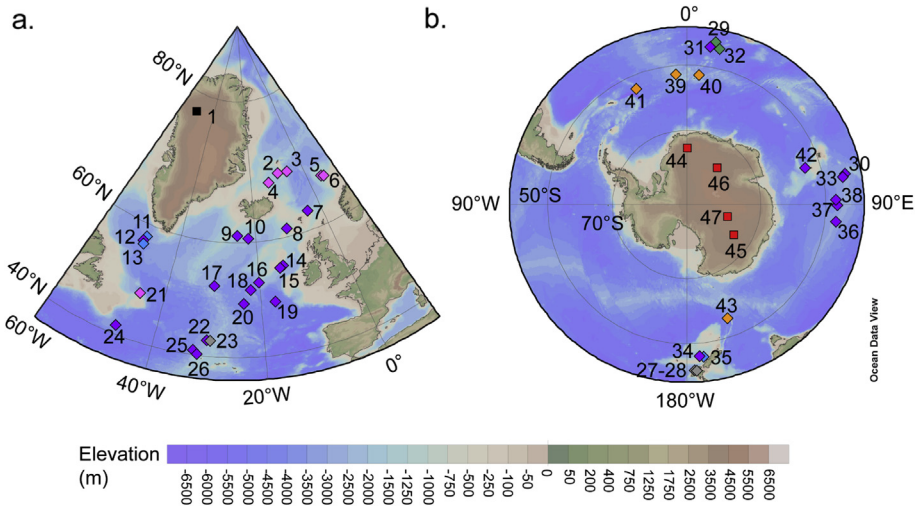

Fig. 1. Location of marine sediment and ice core sites in a. the Northern Hemisphere and b. the Southern Hemisphere included in this study. The compilation contains surface air temperature records from Greenland (black square) and Antarctic (red square) ice cores and SST reconstructions (diamond) based on Mg/Ca (blue), alkenones (grey), diatoms assemblages (orange), radiolarians (green) and foraminifera assemblages (MAT method, purple; NPS percentage, pink). Numbers refer to record labels indicated in Table A1 from the Appendix. (For interpretation of the references to colour in this figure legend, the reader is referred to the web version of this article.)

(EDML), Vostok and Dome F ice cores based on the stable isotopic composition of the ice (Masson-Delmotte et al., 2011b and references therein). Reconstructions of local surface temperature in Antarctic ice cores are based on the present day spatial relationship between the ice isotopic composition of the snow and surface temperature ("isotopic thermometer"). While in principle they should reflect precipitation-weighted temperatures, they are considered here as annual means. Precipitation intermittency, changes in moisture origin as well as site elevation and ice origin changes (Jouzel et al., 2003; Masson-Delmotte et al., 2006; Vinther et al., 2009; Stenni et al., 2010) affect the quantified temperature changes from ice cores. In particular, a modelling study of projected climate and precipitation isotopic composition suggests that using such a method could result in an underestimation of past temperatures for periods warmer than present day conditions (Sime et al., 2009). It results in an uncertainty associated with the different ice-core-based Antarctic absolute temperature reconstructions from ±1 °C to ±2 °C (Stenni et al., 2010; Masson-Delmotte et al., 2011b).

Ice cores retrieved in Greenland are deficient in providing a continuous or/and complete record of the LIG (GRIP members, 1993; Grootes et al., 1993; NorthGRIP community members, 2004; NEEM c. m. 2013). Here, we use the NGRIP $\delta^{18}O_{ice}$ for record alignment purposes between 123 and 110 ka as it represents the only continuous Greenlandic record covering this time interval. In Greenland, isotope–temperature relationships vary through time and have smaller slopes than the modern spatial gradient. We use here the precipitation-weighted temperature estimate corrected for elevation and upstream effects deduced from the NEEM ice core between 116 and 128 ka (NEEM c. m., 2013). Note that while elevation effects are commonly considered to be negligible for Antarctic ice cores (Bradley et al., 2012, 2013), this is not the case for Greenland.

- *Marine sediment cores*:

The marine sediment records included in our data synthesis are mostly located in the North Atlantic region for the Northern Hemisphere and in the Indian and Atlantic sectors of the Southern Ocean for the Southern Hemisphere. The coverage of selected sites reflects the lack of high-resolution SST records covering the LIG in other high-latitude regions and emphasises the need for obtaining future SST records in particular in the Pacific Ocean. SST reconstructions are based on foraminiferal Mg/Ca ratios (three records), alkenone unsaturation ratios (three records) and faunal assemblage transfer functions (24 records based on foraminifera assemblages, two records based on radiolarian assemblages and four records based on diatom assemblages) and the percentage of the polar foraminifera species *Neogloboquadrina pachyderma* sinistral (six records) (Fig. 1, Table A1). Therefore, our data compilation mostly includes SST reconstructions based on faunal assemblages, which reflects the low amount of high-resolution SST records produced with alternative geochemical methods (e.g. alkenone paleothermometry, foraminiferal Mg/Ca) throughout the LIG.

We use these records as representing annual or summer SST as given by the authors of the respective papers. Note that in the case of core MD97-2121, both summer SST (record [27] on Fig. 1 and Table A1, hereafter records are only designated such as [27]) and annual mean SST [28] have been reconstructed from the same source data while for core SU90-08 a summer SST record has been deduced from foraminifera assemblages ([23]; Cortijo, 1995) and an annual SST record has been deduced based on alkenone paleothermometry ([22]; Villanueva et al., 1998). Uncertainties on each reconstructed SST record were estimated from (1) the uncertainty on measurement and (2) the calibration of geochemical and microfossil proxies against modern conditions and range between 0.6 and 2.1 °C depending on the SST proxies (uncertainties for individual records are given in Table A1).

2.2. Strategy for aligning climatic records over the Last Interglacial

Beyond the applicable range of radiocarbon dating, LIG reconstructions benefit from few absolute markers. Large discrepancies of up to several thousand years exist between time scales used to display marine sediment cores and ice core timescales. As an example, Parrenin et al. (2007) report a 2 ka age difference across this time period between the LR04 time scale classically taken as a reference chronology to establish age models of marine sediment cores (Lisiecki and Raymo, 2005) and the EDC3 ice core chronology. Thus, the construction of a common chronostratigraphy between ice core and marine records is critical to compare the LIG climate evolution in both the Northern and Southern Hemispheres.

2.2.1. AICC2012, a new ice core dating and a reference chronology

We use the new AICC2012 ice core chronology (Bazin et al., 2013; Veres et al., 2013) as a reference chronology to display the selected marine sediment and ice core records. The AICC2012 chronology is the first integrated timescale over the LIG, based on a multi-site approach including both Greenland (NGRIP) and Antarctic ice cores (EDC, EDML, TALDICE, Vostok). The new chronology shows only small differences, well within the original uncertainty range, when compared with the EDC3 age scale over the LIG. However, the numerous new stratigraphic links significantly reduce the absolute dating uncertainty down to ±1.6 ka (1σ) over the LIG (Bazin et al., 2013) making it the most appropriate age scale to date with which to compare our synchronised records with model runs and other dated records.

The Dome F and the NEEM ice cores have not been included to construct the AICC2012 chronology (Bazin et al., 2013; Veres et al., 2013). However, both the Dome F and the NEEM ice cores have been previously transferred onto the EDC3 timescale (Parrenin et al., 2007; NEEM c. m., 2013). Thus by using published EDC3-AICC2012 age relationships (Bazin et al., 2013; Veres et al., 2013), we transfer the temperature records from the Dome F and the NEEM ice cores onto the AICC2012 chronology.

2.2.2. Transfer of marine records onto AICC2012

We follow the strategy of Govin et al. (2012) to align marine records onto the AICC2012 ice core chronology. It is based on the assumption that surface-water temperature changes in the sub-Antarctic zone of the Southern Ocean (respectively in the North Atlantic) occurred simultaneously with air temperature variations over inland Antarctica (respectively Greenland). Such a link between air above the polar ice sheets and surrounding surface waters has been observed during the abrupt climate changes over the Last Glacial period and during Termination I which benefit from robust radiocarbon dating constraints (Bond et al., 1993; Calvo et al., 2007). For instance, SST changes at site NA87-22 (^{14}C-dated record, Waelbroeck et al., 2008, 2011) are synchronous within dating uncertainties with both the NorthGRIP $\delta^{18}O_{ice}$ and CH_4 concentration changes over the last 25 ka (Fig. 1 from Masson-Delmotte et al., 2010).

Benthic foraminiferal $\delta^{18}O$ is often used as a stratigraphic tool to place marine records on a common age model (e.g. Lisiecki and Raymo, 2005). We prefer avoiding using this strategy for all the selected marine records since there is evidence for significant offsets (from 1 ka to up to 4 ka) between benthic $\delta^{18}O$ records from different water masses and oceanic basins during deglaciations (e.g. Skinner and Shackleton, 2005; Lisiecki and Raymo, 2009). However, no clear benthic $\delta^{18}O$ offsets (within dating uncertainties, ~2 ka) are observed during the penultimate deglaciation between North Atlantic sites located at different water-depth within the same North Atlantic Deep Water mass (Govin et al., 2012). Therefore, we use benthic foraminiferal $\delta^{18}O$ records to verify the overall agreement of chronologies defined in North Atlantic or Southern Ocean sites located in the same water mass. For this purpose, we use cores MD02-2488 [38] and ODP980 [14] as Southern Ocean and North Atlantic references, respectively, because of the high temporal resolution of their SST records and the availability of multi-proxy records (i.e. planktic and benthic foraminiferal stable isotopes).

To align marine sediment cores onto the AICC2012 chronology, we use the software AnalySeries 2.0 (Paillard et al., 1996) and define the minimum number of tie points which produces the best possible alignment. Age models are constructed by linear interpolation (i.e. constant sedimentation rate) between tie-points. The relative uncertainty attached to each tie point is graphically estimated through multiple alignment possibilities. It takes into account the time resolution of the records used to perform the alignment and reflects how robust the tie-point is regarding its location (e.g. situated at the mid-point of a well-marked transition) and how synchronous the records used for the alignment become after defining the tie-point. A list of defined tie-points, corresponding rationale and relative 1σ age uncertainties on the AICC2012 timescale is given for every selected sediment core in Table A2.

- *Southern Ocean cores*: We align each SST record from the Southern Ocean onto the EDC deuterium record (δD, Jouzel et al., 2007; site [45] on Fig. 1) displayed on AICC2012. Our decision to align marine cores from all Southern Ocean sectors onto the EDC record is justified by the fact that the Dome F, EDML and EDC water stable isotope records show similar variations, with approximately simultaneous climatic transitions (Masson-Delmotte et al., 2011b). Also considering either the EDC δD record or the EDC site temperature estimate as a reference curve for aligning marine sediment records onto AICC2012 does not affect the timing of the glacial inception and the start of Termination II (Masson-Delmotte et al., 2011b). Termination II is slightly more abrupt in the site temperature record than in the δD record but it only leads to an age difference for the two corresponding mid slope points of less than 500 years.

Fig. 2 (left panel) illustrates the alignment of core MD88-769 [37] onto AICC2012 based on four tie points. We define a first tie point by aligning the first SST increase with the EDC δD increase at the beginning of Termination II (138.2 ± 2 ka). Then, we define a mid-slope tie point in the course of the glacial–interglacial transition (131.4 ± 1 ka) and another mid-slope tie point during the glacial inception (116 ± 1.5 ka). Finally, a last relative age constraint is determined by tying the mid-slope of the δD increase corresponding to the Antarctic Isotopic Maxima 24 and its counterpart identified in the SST record (106.7 ± 2 ka). We are confident in our alignment since it results in simultaneous benthic $\delta^{18}O$ variations recorded in cores MD88-769 and MD02-2488 [38] (which was retrieved at a similar water depth and previously transferred onto AICC2012 following a similar strategy) (Fig. 2, left panel).

- *North Atlantic cores*: We align the SST proxy records from the North Atlantic cores to the ice $\delta^{18}O$ record from the NGRIP Greenland ice core during the Last Glacial inception. We favour the NGRIP ice core to the NEEM ice core as the Greenland reference ice core because (1) the NGRIP ice core is one of the ice records used to constrain the AICC2012 chronology and (2) the NGRIP ice core represents a continuous record up to 123 ka (NorthGRIP c. m. 2004) while the NEEM ice core record presents stratigraphic discontinuities at the end of the LIG (NEEM c. m. 2013). Since the NGRIP ice core does not cover the early LIG, alternative strategies are followed to align marine and ice core records prior to 122 ka. First, we assume that the global abrupt methane increase during Termination II reflects synchronous abrupt warming of the air above Greenland. This is indeed observed during Termination I as well as during millennial-scale Dansgaard–Oeschger events (e.g. Chappellaz et al., 1993; Huber et al., 2006; Baumgartner et al., 2013). On Fig. 2, the right panel illustrates the alignment of core SU90-44 [19] onto AICC2012 using four tie-points. The beginning of the LIG is relatively well constrained in all North Atlantic cores with a tie point linking the final SST increase with the abrupt methane increase recorded in the EDC ice core (128.7 ± 0.5 ka). However, in order to constrain the 130 ka time slice, it is necessary to define a tie point prior to 131 ka (see Section 2.3). Thus, we define a first tie point during the preceding glacial period using the assumption that the establishment of the very cold glacial conditions related

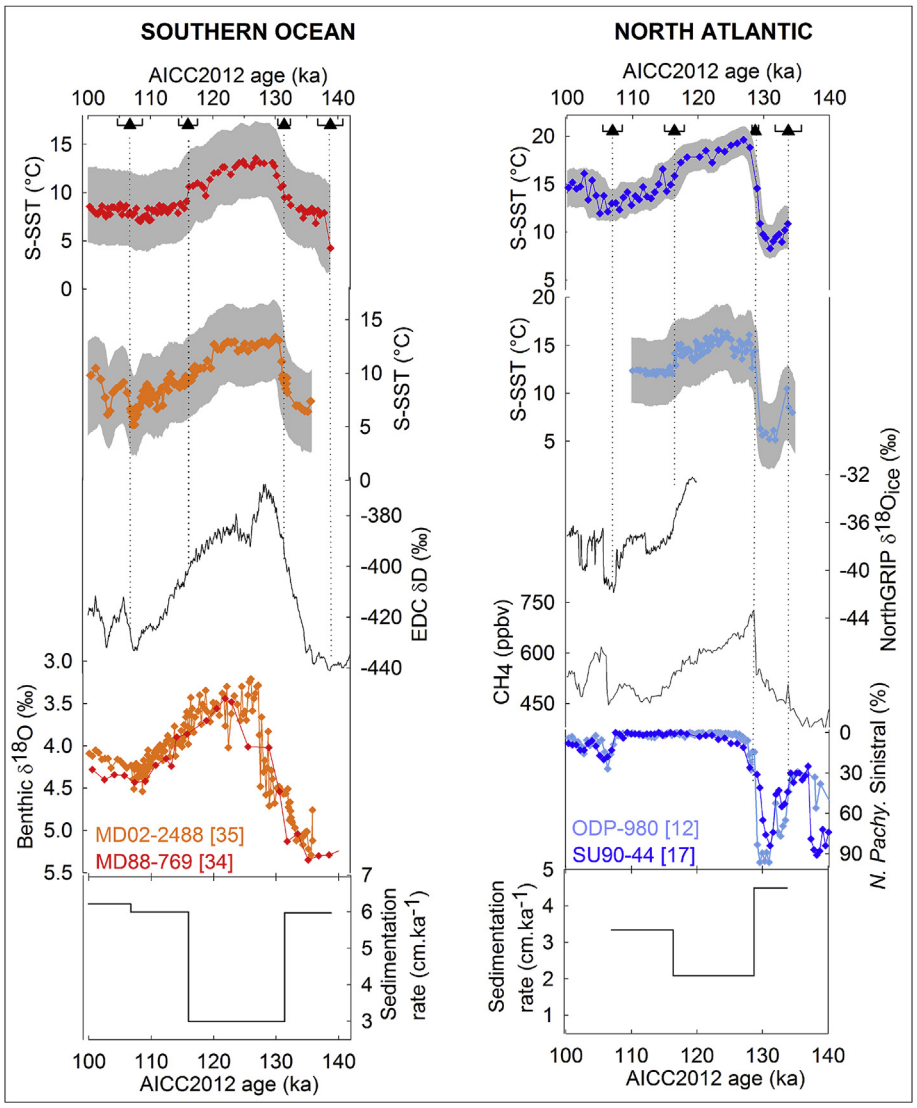

Fig. 2. Definition of age models in the Southern Ocean MD88-769 core [34] (red curves) and the North Atlantic SU90-44 core [17] (blue curves). Numbers between brackets correspond to of the core location on Fig. 1. Triangles (with error bars representing associated relative 1σ dating uncertainties) and vertical dotted lines highlight the tie-points defined between *(left panel)* the MD88-769 Summer SST record and the Antarctic EDC δD record (Jouzel et al., 2007; black) and *(right panel)* between the SU90-44 Summer SST record and the NGRIP ice $\delta^{18}O$ record (NorthGRIP c. m. 2004; black), the CH_4 concentration measured in the air trapped in the EDC ice core (Loulergue et al., 2008; grey) and the percentages of *N. pachyderma* sinistral (LSCE database). The resulting agreement between Summer SST and benthic $\delta^{18}O$ records from MD88-769 and MD02-2488 (Govin et al., 2012; grey) both displayed on AICC2012 is shown as well as resulting sedimentation rate variations and associated relative age uncertainty of the tie points for each core. Grey shaded areas mark non-parametric 2σ (2.5th and 97.5th percentiles) confidence intervals of Monte Carlo iterations (see text for details). (For interpretation of the references to colour in this figure legend, the reader is referred to the web version of this article.)

to Heinrich event 11 is synchronous within the North Atlantic region. As a result, we tie the increase of the percentage of *N. pachyderma* sinistral in core SU90-44 with the one recorded at 133.8 ±2 ka in core ODP980 previously transferred onto AICC2012 (Table A2). Then, at the end of the LIG, the first pronounced North Atlantic cooling is tied to the corresponding enhanced cooling in the NGRIP ice core (116.8 ± 1.5 ka). We finally define a tie point that links SST and Greenland air temperature at the end of the first abrupt event, Dansgaard–Oeschger 25 (107.3 ± 1.5 ka). We are confident in the choice of these tie points since they lead to simultaneous increases in the percentage of *N. pachyderma* sinistral recorded in cores SU90-44 and ODP980 (Fig. 2, right panel). A similar procedure is followed for all other North Atlantic high latitude sites except for the site EW9302-JPC2 [21] located in the Labrador Sea and for which it is less straightforward to define the alignment onto AICC2012. Note that in the rest of the manuscript, we differentiate the North Atlantic high latitude region from the Labrador Sea area.

- *Nordic Seas and Labrador Sea cores*: Climatic alignments of records retrieved in the Labrador Sea and the Nordic Seas are more equivocal for two main reasons. First, most of the SST estimates have been derived from the percentage of *N. pachyderma* sinistral which is not suitable to record SST variations below 6.5 °C (Tolderlund and Be, 1971; Kohfeld et al., 1996). Indeed, while the percentage of this species is linearly related to SST changes for water of ~6.5–15 °C, the abundance of *N. pachyderma* sinistral already accounts for ~95% of foraminifera faunal assemblages at 6.5 °C, thus any temperature change below this value cannot be tracked with this method (Kohfeld et al., 1996; Govin et al., 2012). Also, potential issues in the preservation of the planktic foraminifera shells may affect

the SST reconstructions (e.g. Zamelczyk et al., 2012). Unfortunately to our knowledge, there are very few alternative quantitative SST estimates available for the LIG in the Labrador Sea (only [11], [12], [13] and [21]) and in the Nordic Seas (only [7]) based on alternative SST reconstruction methods.

Second, planktic and benthic foraminiferal $\delta^{18}O$ are characterised by highly depleted $\delta^{18}O$ values during Termination II (e.g. Risebrobakken et al., 2006; Bauch and Erlenkeuser, 2008), which makes the identification of the LIG climatic optimum in foraminiferal stable isotopes difficult. Very low benthic $\delta^{18}O$ during Termination II may derive from intensified sea ice formation and brine rejection that transferred to bottom waters the low $\delta^{18}O$ signal recorded in surface waters in response to strong iceberg melting (e.g. Risebrobakken et al., 2006). Alternatively, Bauch and Bauch (2001) proposed that such low benthic $\delta^{18}O$ values may reflect the warming of bottom waters in response to the inflow of warm subsurface Atlantic waters below fresh and stratified surface waters in the Nordic Seas.

To overcome these difficulties, we combine here several lines of evidence (i.e. temperature variations, tephra layers, foraminiferal stable isotopes, biostratigraphic constraints) to define chronologies as robust as possible in the Norwegian and Labrador Seas. The difficulty of performing these alignments is reflected in the relatively high relative dating uncertainties associated to each tie point (Table A2). In three of these high northern latitude sites, temperature anomalies cannot be reconstructed for the 130 and 115 ka data-based time slices due to the lack of chronological constraints. We update the chronology that was originally defined in the Labrador Sea core EW9302-JPC2 using the EDC3 timescale as a reference by Govin et al. (2012) in order to transfer the records onto AICC2012. Fig. 3 illustrates how we transfer MD95-2009 [7] and HM71-19 [2] records from the Nordic Seas onto the AICC2012 chronology. First, the North Atlantic core ENAM33 [8] is transferred onto AICC2012 via the alignment of its SST record (Rasmussen et al., 2003; this study; Details are given on the SST reconstruction method in the appendix) to the NGRIP $\delta^{18}O_{ice}$ and the EDC CH_4 concentration (see previous section for details on the approach). Second, we define stratigraphic links between core ENAM33 and the Nordic sea core MD95-2009 to transfer the latter onto AICC2012. A first tie point is determined based on the alignment of MD95-2009 benthic $\delta^{18}O$ record with core ODP980 at 138.2 ka associated with a relative age uncertainty of 4 ka. Such a relative age uncertainty takes into account the difficulty in defining the tie point and the possible time lags between two benthic $\delta^{18}O$ records from different oceanic basins. Then, we

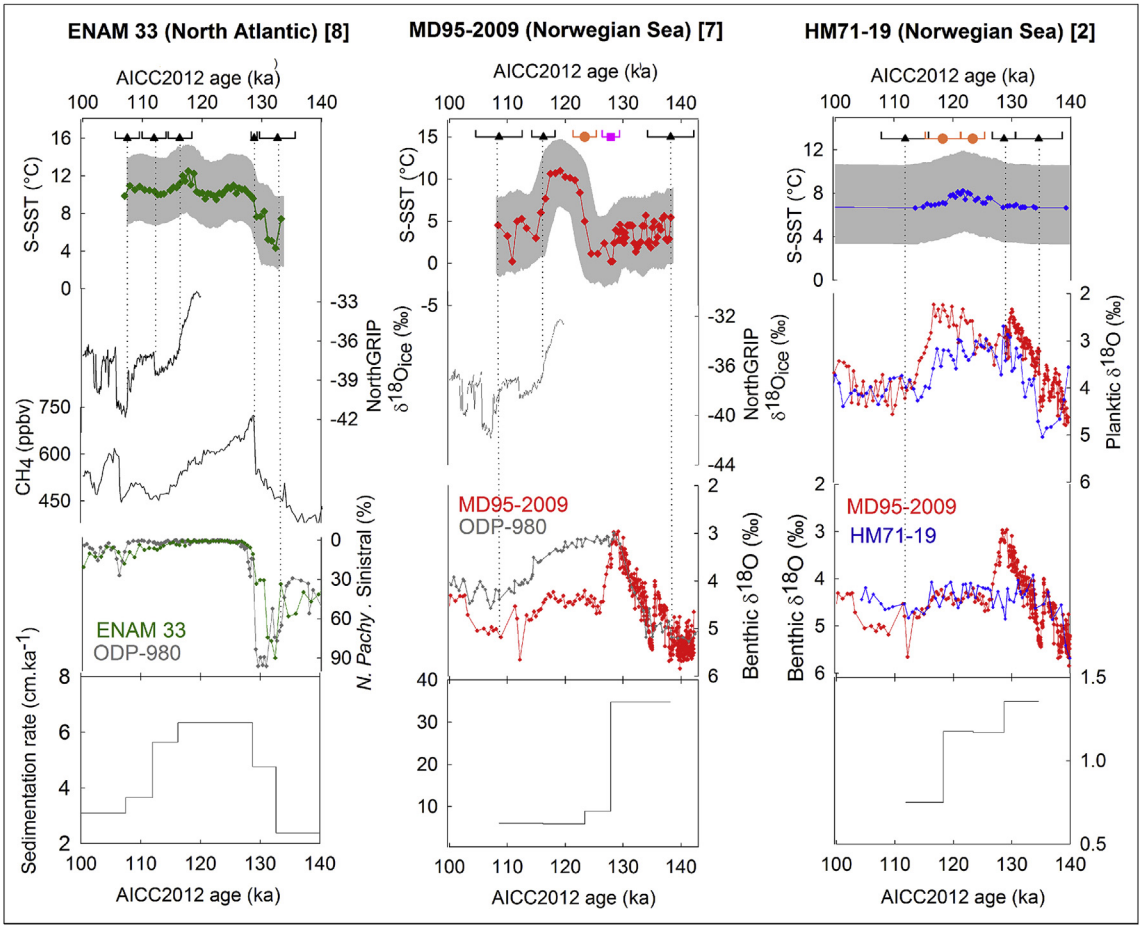

Fig. 3. Definition of age models in one North Atlantic (ENAM33 [8], green curves) and two Norwegian Sea sediment cores (MD95-2009 [7] and HM71-19 [2]). Numbers between brackets correspond to the location of records on Fig. 1. ENAM33 core has been first transferred onto AICC2012 through climatic alignments (tie points indicated in black triangles). In addition to climatic alignment-based tie points (black triangles and pink square for the tie point proposed by Rasmussen et al., 2003), core MD95-2009 was linked to core ENAM33 thanks to the ash layer 5e-Low/bas-IV identified in both cores (orange dot). Core HM71-19 was aligned onto core MD95-2009 based on the ash layers 5e-Midt/RHY and 5e-Low/bas-IV identified in both cores (orange dots) and planktic and benthic $\delta^{18}O$ records (black triangles). Sedimentation rate variations and defined relative age uncertainty are also shown for each core. Grey shaded areas mark non-parametric 2σ (2.5th and 97.5th percentiles) confidence intervals of Monte Carlo iterations (see text for details). (For interpretation of the references to colour in this figure legend, the reader is referred to the web version of this article.)

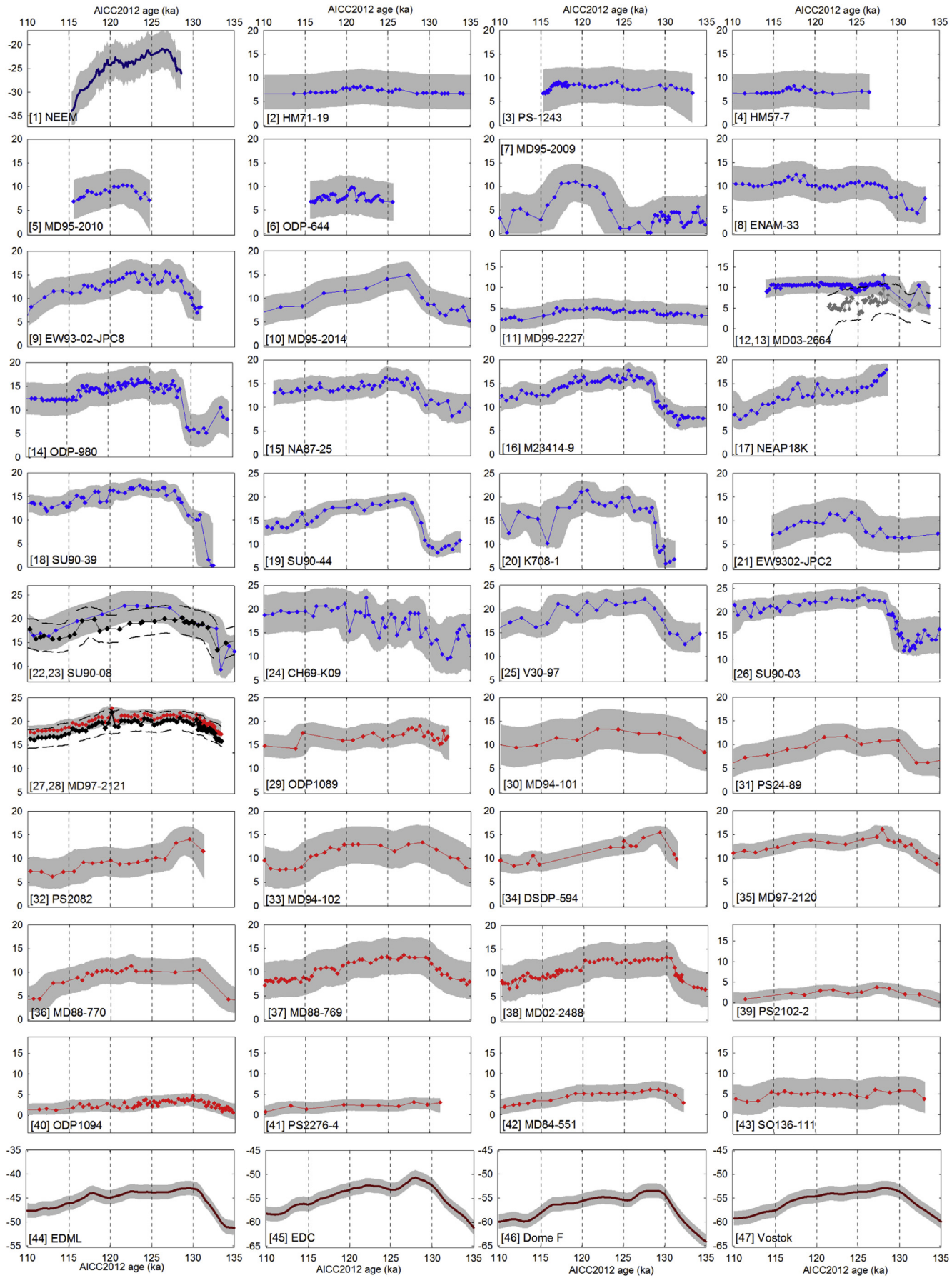
AICC2012 age (ka)
[1] NEEM
[2] HM71-19
[3] PS-1243
[4] HM57-7
[5] MD95-2010
[6] ODP-644
[7] MD95-2009
[8] ENAM-33
[9] EW93-02-JPC8
[10] MD95-2014
[11] MD99-2227
[12,13] MD03-2664
[14] ODP-980
[15] NA87-25
[16] M23414-9
[17] NEAP18K
[18] SU90-39
[19] SU90-44
[20] K708-1
[21] EW9302-JPC2
[22,23] SU90-08
[24] CH69-K09
[25] V30-97
[26] SU90-03
[27,28] MD97-2121
[29] ODP1089
[30] MD94-101
[31] PS24-89
[32] PS2082
[33] MD94-102
[34] DSDP-594
[35] MD97-2120
[36] MD88-770
[37] MD88-769
[38] MD02-2488
[39] PS2102-2
[40] ODP1094
[41] PS2276-4
[42] MD84-551
[43] SO136-111
[44] EDML
[45] EDC
[46] Dome F
[47] Vostok

include the biostratigraphic link proposed by Rasmussen et al. (2003) between cores MD95-2009 and ENAM33 dated at 128.0 ± 1.5 ka on AICC2012. These authors aligned in both cores the disappearance of Atlantic benthic foraminifera species groups that are replaced by benthic species associated with the cold Norwegian Sea Overflow Water, hereby reflecting the onset of convection in the Nordic seas (Rasmussen et al., 2003). We use also as a stratigraphic link the ash layer 5e-Low/BasIV identified in both ENAM33 and MD95-2009 cores (Rasmussen et al., 2003). While an older age was reported by Rasmussen et al. (2003) based on a correlation onto the SPECMAP time scale, the ash layer 5e-Low/BasIV in core ENAM33 corresponds to a depth level dated at 123.7 ± 2 ka based on the depth–age relationship resulting from the alignment of this core onto AICC2012 (Fig. 3, left panel). Thus, this age of 123.7 ± 2 ka is used as a third tie point to constrain the age model of core MD95-2009 (Fig. 3, middle panel). At the end of the LIG, the pronounced cooling in MD95-2009 SST record is tied to the corresponding enhanced cooling in the NGRIP ice core at 116.7 ± 2 ka. A final tie point at 107.5 ± 4 ka is determined based on the alignment of MD95-2009 benthic $\delta^{18}O$ record with core ODP980.

We use two types of tie-points to transfer core HM71-19 from the Nordic Seas onto the AICC2012 timescale. First, the tephra layers 5e-Low/BasIV and 5e-Midt/RHY (Fronval et al., 1998; Rasmussen et al., 2003) dated at 123.7 ± 2 ka and 118.9 ± 3 ka on AICC2012 and identified in both cores HM71-19 and MD95-2009 (Fronval et al., 1998; Rasmussen et al., 2003) are used as two tie points. Note that to define the age of 118.9 ± 3 ka for the tephra layer 5e-Midt/RHY, we follow the same strategy as for the tephra layer 5e-Low/BasIV, i.e. the age is deduced based on the depth/age relationship for core MD95-2009 transferred onto AICC2012. As a result, uncertainties associated to these tie points include the uncertainty linked to the respective estimated ages of 5e-Low/basIV and 5e-Midt/RHY as defined in cores ENAM33 and MD95-2009, respectively, transferred onto the AICC2012 timescale. Second, in order to provide additional constraints at the onset and demise of the LIG, we also align the planktic $\delta^{18}O$ record (tie points at 134.6 ± 4 ka and 128.7 ± 2 ka) and benthic $\delta^{18}O$ record (112.5 ± 4 ka) from core HM71-19 onto those from the Norwegian Sea core MD95-2009. Indeed, we make the assumption that at the scale of glacial–interglacial changes, hydrological changes within the Nordic Seas are occurring at the same time within an uncertainty of a few thousand years based on existing records (e.g. Bauch et al., 2000; Bauch et al., 2012).

For each marine sediment record, we perform a Monte-Carlo analysis to propagate the errors associated with both (1) the uncertainty linked to the SST reconstruction method and (2) the age uncertainties on the tie points that we defined during the record alignment. The error on the SST reconstruction is set to the value attributed for each SST record in its original publication (listed in Table A1). It varies from 0.6 °C to up to 2.1 °C and it is on average 1.4 °C. To include uncertainties linked to the temporal alignment of records, we first estimate dating uncertainties associated with defined tie-points (Table A2). Second, we propagated these errors by applying to all cores a Monte-Carlo analysis performed with 1000 age model simulations. For every iteration, we add random noise to SST values within the space of temperature reconstruction error. Third, we (1) randomly determined the age of every tie-point within the space of dating error documented in Table A2, (2) checked for potential age reversals and discarded the iteration in those cases, (3) assigned an age to every depth with SST values by linear interpolation between tie-points. On Figs. 2–4, we show SST records associated with a non-parametric 2σ confidence interval envelope (from the 2.5th to the 97.5th percentiles after resampling every 0.1 ka).

2.3. Establishment of data-based time slices at 130 ka, 125 ka, 120 ka and 115 ka

In order to provide a dynamical climatic description not only of the LIG climatic optimum (e.g. Turney and Jones, 2010; McKay et al., 2011) but also covering of its onset and demise, we choose to calculate temperature anomalies for four time windows: 114–116, 119–121, 124–126 and 129–131 ka, hereafter referred to as the data-based 115, 120, 125 and 130 ka time slices, respectively. Although, snapshot simulations have also been run for the 128 and 126 ka climatic conditions, we consider that the average relative age uncertainties associated with the alignment of marine cores onto AICC2012 prevent us to propose more that 4 time slices within the 115 ka–130 ka time interval. Also, we choose a 2 ka time window for each time slice so that each average temperature anomaly relies on a sufficient number of data points. To develop a comparison to present-day summer SST, mean annual or summer SST for each marine core location are extracted at 10 m depth from the 1998 World Ocean Atlas (WOA98), as recommended in Kucera et al. (2005) (Table A1). Summer SST are defined as averaged SST during the months of July, August and September for the Northern Hemisphere (JAS SST) and as the averaged SST during the months of January, February and March for the Southern Hemisphere (JFM SST). Note that the choice of the WOA database has a negligible impact on the resulting SST anomalies. A root-mean-standard-deviation of only 0.2 °C is deduced from a comparison of JAS present-day summer SST at all marine core locations from WOA98, WOA2001, WOA2005, WOA2009, and WOA2013. In line with MARGO community members (2009), we neglect here the uncertainty on modern WOA98 SST, which we consider to be much smaller than the error on reconstructed SST. For ice core records, we use annual mean surface air temperature given in the literature based on present day instrumental temperature measurements (Masson-Delmotte et al., 2011b; NEEM c. m., 2013).

For each marine sediment record, we use the Monte-Carlo analysis to determine the temperature anomalies and associated temperature uncertainty for each time slice. Mean SST anomalies for each time window were calculated after resampling every 0.1 ka. From the 1000 slightly different SST anomalies obtained for each time slice, the median SST anomaly and the associated non-parametric 2σ uncertainties (2.5th and 97.5th percentiles) were calculated (Fig. 5). The uncertainty on temperature anomalies is ± 2.6 °C on average. It increases for the time slices 115 and 130 ka since they are within large climatic transitions. As a result, even small dating uncertainties can lead to larger differences in temperature anomalies deduced for one given time slice from the various Monte Carlo simulations.

Fig. 4. Air and summer sea surface temperature records displayed on the AICC2012 timescale between 110 ka and 135 ka (red colours for the Southern Hemisphere records and blue colours for the Northern Hemisphere records). Note that *y* axes display the same temperature amplitude of 20 °C to allow visual comparison between sites. Grey shaded areas mark non-parametric 2σ (2.5th and 97.5th percentiles) confidence intervals of Monte Carlo iterations (see text). Note that two SST records have been produced for sites MD03-2664 [12, 13], SU90-08 [22, 23] and MD-2121 [27, 28]. Annual signals [22, 28] are displayed in black and spring signal is displayed in grey. Dashed black lines mark their non-parametric 2σ (2.5th and 97.5th percentiles) confidence intervals of Monte Carlo iterations (see text). (For interpretation of the references to colour in this figure legend, the reader is referred to the web version of this article.)

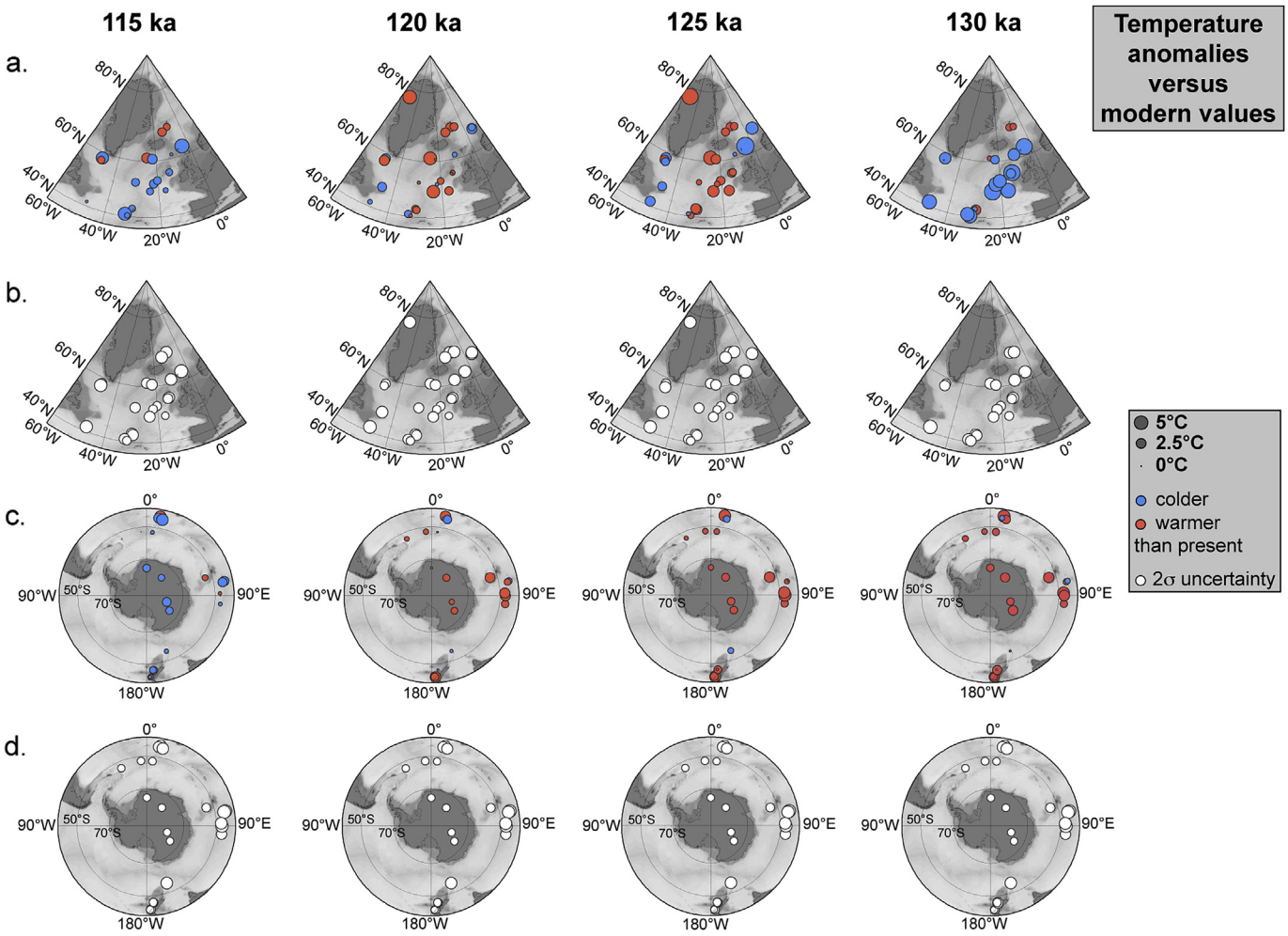

Fig. 5. Temperature anomalies estimated for four time-slices at 115 ka, 120 ka, 125 ka and 130 ka. a. Northern Hemisphere air temperature and SST anomalies. SST anomalies are calculated relative to modern summer SST taken at 10 m water-depth from the World Ocean Atlas 1998 (following the MARGO recommendations, Kucera et al., 2005, months used to estimate modern SST at site locations are July, August and September). b. 2σ uncertainties of temperature anomalies in the Northern Hemisphere taking into account the error on the temperature reconstruction and the propagated dating errors. c and d. Same as a. and b. for the Southern Hemisphere. Summer months used to estimate modern SST at site locations are January, February and March. The bigger the dot is, the larger the anomaly is. Warming (cooling) vs modern temperature is represented in orange (blue).

2.4. Model simulations

To illustrate the potential of our new LIG data synthesis in model-data comparisons, we use two snapshot simulations at 125 ka and 130 ka performed with two fully coupled global atmosphere-land surface-ocean-sea ice general circulation models (GCM): the Community Climate System Model, Version 3 (CCSM3, Collins et al., 2006) and the HadCM3 MOSES 2.1 model (Gordon et al., 2000). These two GCMs have been previously used to simulate the LIG and pre-industrial climates and details on the model components and the methodology of coupling are given by Otto-Bliesner et al. (2013) and Lunt et al. (2013) respectively. Whilst biases in SST estimates arise in climate models for several reasons including poor representations of sea ice variability and the Atlantic Meridional Overturning Circulation, Lunt et al. (2013) have shown that CCSM3 and HadCM3 models have the best skill (or smallest error) for the simulation of pre-industrial surface air temperature, as compared to the NCEP climatology within all models used to simulate the LIG period.

Boundary conditions are summarised in Table 1. The Earth's orbital configuration constitutes the dominant forcing for the 125 ka and 130 ka climate compared with pre-industrial conditions. CCSM3 climatologies are calculated from the last 30 years of a 950 year-long pre-industrial simulation and of 350 year-long simulations at 125 and 130 ka (continued from previously run LIG simulations). HadCM3 climatologies are calculated from the last 50 years of a >1000 year pre-industrial simulation and the last 50 years of 550 year-long simulations at 125 and 130 ka. The lengths of the two simulations are different because they result at first from independent initiatives but in both cases, the surface diagnostics are in reasonable equilibrium with the modified climate although neither model has reached equilibrium in the deep ocean. For the preindustrial CCSM3 shows trends of less than 0.1 °C per century in the Southern Ocean while HadCM3 shows a trend of 0.02 °C per century for summer SST at high southern latitudes. In order to compare the model temperature anomalies for the defined data-based time slices, it is necessary to account for the discrepancy between the pre-industrial reference used for the model and the modern reference used for the data. To correct for this effect, we calculate the difference between the gridded NODC WOA98 dataset (representative of the modern reference) and the gridded HadISST dataset (Rayner et al., 2003) (representative of a pre-industrial [1870–1899 AD] reference) and add this to the model anomaly (LIG minus pre-industrial). The average correction at the core

Table 1
Forcing and boundary conditions used in CCSM3 and HadCM3 simulations (Otto-Bliesner et al., 2013; Lunt et al., 2013 for more details). Greenhouse gas concentrations used for the HadCM3 simulations are those specified by PMIP3. They were deduced from records measured on the EDC ice core displayed on the EDC3 timescale (Spahni et al., 2005; Loulergue et al., 2008; Lüthi et al., 2008). Similar values are obtained when using the AICC2012 time scale. Greenhouse gas concentrations used for the CCSM3 simulations are higher than the ones taken in the PMIP3 LIG protocols. They were deduced from the EDC greenhouse gas concentration records displayed on the EDC3 timescale but represent the peak overshoot values occurring at 128–129 ka.

	CCSM3			HadCM3		
	130 ka	125 ka	PI	130 ka	125 ka	PI
Geography	Modern	Modern	Modern	Modern	Modern	Modern
Ice Sheets	Modern	Modern	Modern	Modern	Modern	Modern
Vegetation	Modern	Modern	Modern	Modern	Modern	Modern
CO_2 (ppmv)	300	273	289	257	276	280
CH_4 (ppbv)	720	642	901	512	640	760
N_2O (ppbv)	311	311	281	239	266	270
Solar constant ($W\ m^{-2}$)	1367	1367	1365	1365	1365	1365
Orbital	130 ka	125 ka	1990	130 ka	125 ka	1950

locations is of 0.44 °C. Similar to the calculations of temperature anomalies in marine records (Section 2.3), we show here simulated summer SST anomalies defined as JAS for the Northern Hemisphere and JFM for the Southern Hemisphere. For polar ice cores, we consider annual temperature anomalies at the locations of the Antarctic ice cores and the precipitation-weighted temperature anomaly at the location of the NEEM Greenlandic ice core (Figs. 6–7).

3. Results

3.1. LIG timeseries

The evolution of synchronised surface air and sea surface temperature records over the LIG (Fig. 4) highlights several major features. We highlight an asynchronous establishment of peak interglacial temperatures between the two hemispheres across the LIG by calculating the average date at which the maximum LIG temperature peaks occurs for the Southern Hemisphere records on one side (Fig. 4; records [27]–[47]; note that when a maximum value was not clearly identified in the record, we took the date where a clear change of slope is marked) and for the North Atlantic high latitude region records on the other side (Fig. 4; records [10] and [14]–[26], excluding the record from site CH69-K09 [24] for which it is difficult to unambiguously identify a temperature maximum). For the Southern hemisphere records, we obtain a date of 129.3 ka associated with a standard deviation of 0.9 ka while we obtain a younger date of 126.4 ka associated with a standard deviation of 1.9 ka for the North Atlantic high latitude records. This result hence illustrates the hemispheric differences highlighted in our database. Air temperature maximum conditions at the NEEM site [1] in Greenland occur at 126.9 ka, synchronously within dating uncertainties with the warmest conditions in the North Atlantic high latitudes. Although concerns about the synchronisation precluded our use of European vegetation data here, we note that the time of maximum temperature (in both the warmest and coldest month) across Europe was also deduced to be around 127 ka (Brewer et al., 2008). In the Nordic Seas, SST records (records [2]–[7]) are characterised by small amplitude temperature changes across the LIG, in particular because of the limitation of *N. pachyderma* sinistral percentages to record STT variations at low temperatures (see Section 2.2). Because the temperature uncertainty associated with each record after being aligned onto AICC2012 is about 3–4 °C, it is difficult to determine with confidence the timing of maximum surface temperature peaks in this region. No significant maximum temperature peak is identified in records [2], [3], and [4] located at the highest latitudes (between 68°N and 70°N; Fig. 4). Still, the establishment of interglacial temperature seems to occur at 122.5 ka, and 122.7 ka in MD95-2009 [7] and MD95-2010 [5] respectively. In the Labrador Sea, records [11] and [12] do not record unambiguously a temperature maximum while a LIG temperature peak is identified at 124.4 ka in record [21].

Our data synthesis also reveals large regional climatic variability, in particular in the North Atlantic high latitude region. For example, the summer SST record from core MD95-2014 exhibits a deglacial temperature increase toward a maximum, directly followed by a smooth temperature decrease (Fig. 4, [10]). At other sites, such as the coring sites of ENAM33 and ODP980, maximum summer SSTs prevail for 7–13 ka before cooling and glacial inception take place (Fig. 4, [8] and [14]). Also M23414-9 and SU90-39 SST records clearly exhibit a two-step deglaciation interrupted at 130 ka (Fig. 4, [16] and [18]). Such a pattern has also been recently shown and discussed in a new SST record from the Alboran Sea located at 36°12.3′N (core ODP976; Martrat et al., 2014) while this is not a feature that is unambiguously observed in the other records included in our synthesis (located above 40°N). However, the likelihood of recording such a millennial-scale feature is highly dependent on the temporal resolution of the records. Regional variability is observed in the Southern Hemisphere with a clear temperature overshoot in Antarctic surface air temperature records (records [44]–[47]) and possibly in DSDP-594 [34]. This overshoot is not visible in other Southern Ocean marine records.

Finally, our synthesis suggests a larger magnitude of temperature changes over Antarctica (3.5 °C temperature change on average in ice core records between 130 and 115 ka) than at the surface of the surrounding Southern Ocean. Contrasts are also observed within the Southern Ocean with marine records at the highest latitudes (up to 50°S) showing a smaller amplitude of temperature change between 130 and 115 ka (1.2 °C on average) than for marine records north of 50°S (2.5 °C on average). Similarly, Nordic Seas records north of 67°N only exhibit less than a 2 °C amplitude in the temperature change while MD95-2009 [7] records up to a 10 °C temperature change over Termination II. However, because SST variations below 6.5 °C are not well captured by the percentages of the polar species *N. pachyderma* sinistral (Govin et al., 2012), the amplitude of temperature changes may be underestimated in the Nordic Seas. Still, overall the strongest amplitudes of temperature changes are recorded in the Northern Hemisphere high latitudes compared to the Southern Hemisphere high latitudes (e.g. SU90-39 [18] and SU90-08 [22]).

3.2. LIG data-based time slices

Our four data-based time slices capture the major features characterising the spatial sequence of events described in Section 3.1 (Fig. 5). In particular, the 130 ka time slice clearly illustrates the asynchrony previously reported between the Northern and the Southern Hemisphere high latitudes (e.g. Masson-Delmotte et al., 2010; Govin et al., 2012). It also reveals SST significantly cooler-than-present-day sea surface conditions (e.g. up to 7.5 ± 3 °C cooler for [20]) in the high latitudes of the Northern Hemisphere while temperatures were slightly warmer than today (1.7 ± 2.5 °C on average) in most of the Southern Hemisphere sites.

Warmer than present day climatic conditions are visible on the 130, 125 and 120 ka time slices in the Southern Hemisphere, while

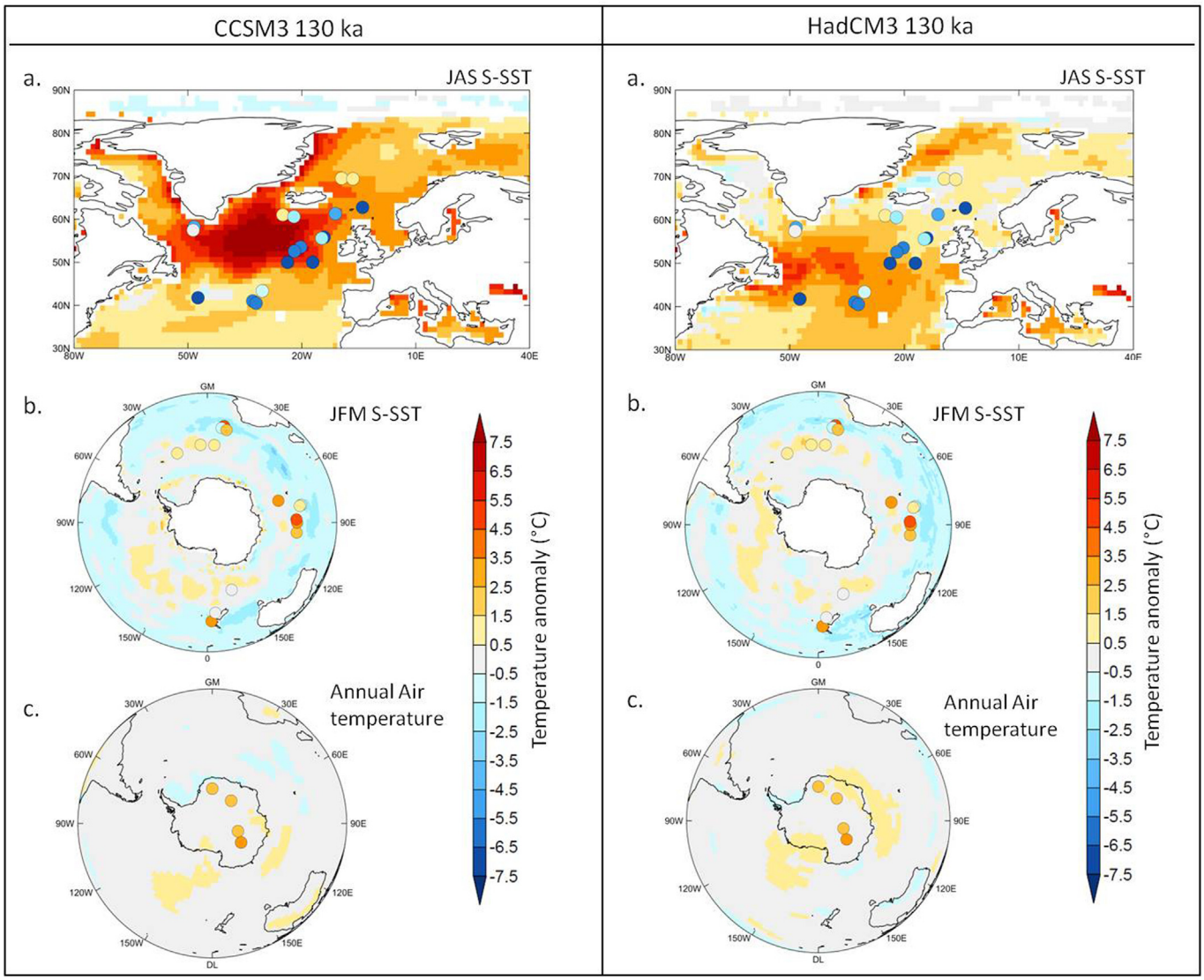

Fig. 6. 130 ka Model-data comparison for the time slice at 130 ka, using the (left panel) CCSM3 and (right panel) HadCM3 models. a. Summer SST temperature anomalies from the marine sediment data (dots) superimposed onto model July–August–September SST simulation in the Northern Hemisphere; b. Summer SST temperature anomalies from the marine sediment data (dots) superimposed onto the model January–February–March SST simulation in the Southern Ocean; c. Annual surface air temperature anomalies from the ice core data (dots) superimposed onto the model annual simulation.

they are only unambiguously observed on the 125 and 120 ka data-based time slices in the Northern Hemisphere.

3.3. Model-data comparison at 130 ka and 125 ka

Figs. 6 and 7 display the model-data comparison for the 130 ka time-slice and the 125 ka time slice respectively. Absolute dating should be considered when comparing our new LIG synthesis to model outputs. Because the data-based time slices represent 2 ka time windows that have been calculated every 5 ka from 130 to 115 ka, dating errors affecting the palaeoclimatic records uncertainties (including the absolute dating error of the AICC2012 time scale, i.e. less than 1.6 ka during the LIG, Bazin et al., 2013) should have a limited impact on the main patterns highlighted in the model-data comparison.

In the Northern Hemisphere high latitudes, both the HadCM3 and CCSM3 simulations exhibit at 130 ka significantly warmer summer sea surface conditions compared to present-day. In contrast, reconstructed summer temperatures display cooler conditions compared to present day. Note also that the CCSM3 130 ka simulation is warmer than the HadCM3 130 ka simulation. This is predominantly due to the difference in GHG concentration values used where CCSM3 has a CO_2 value ~50 ppmv higher than HadCM3, though also influenced by the different sea ice sensitivities of the two models (Table 1).

In the Southern Ocean, the discrepancy between simulated and reconstructed summer SST is smaller than in the Northern Hemisphere high latitudes. Still, LIG modelled summer SST are similar to present-day ones in both model simulations while the data from the Southern Ocean illustrate surface oceanic conditions warmer by to up to 3.9 ± 2.8 °C compared to present day (i.e. [29]). Modelled annual air temperatures above Antarctica are similar to present-day at 130 ka in both CCSM3 and HadCM3 simulations. However, all reconstructions from Antarctic ice cores suggest temperatures 1.5 ± 1.5 °C–2.5 ± 1.5 °C warmer than for present-day. Thus, our model-data comparison at 130 ka illustrates that these two models correctly simulate neither the cooler-than-present-day conditions in the northern high latitudes nor the warmer-than-present-day

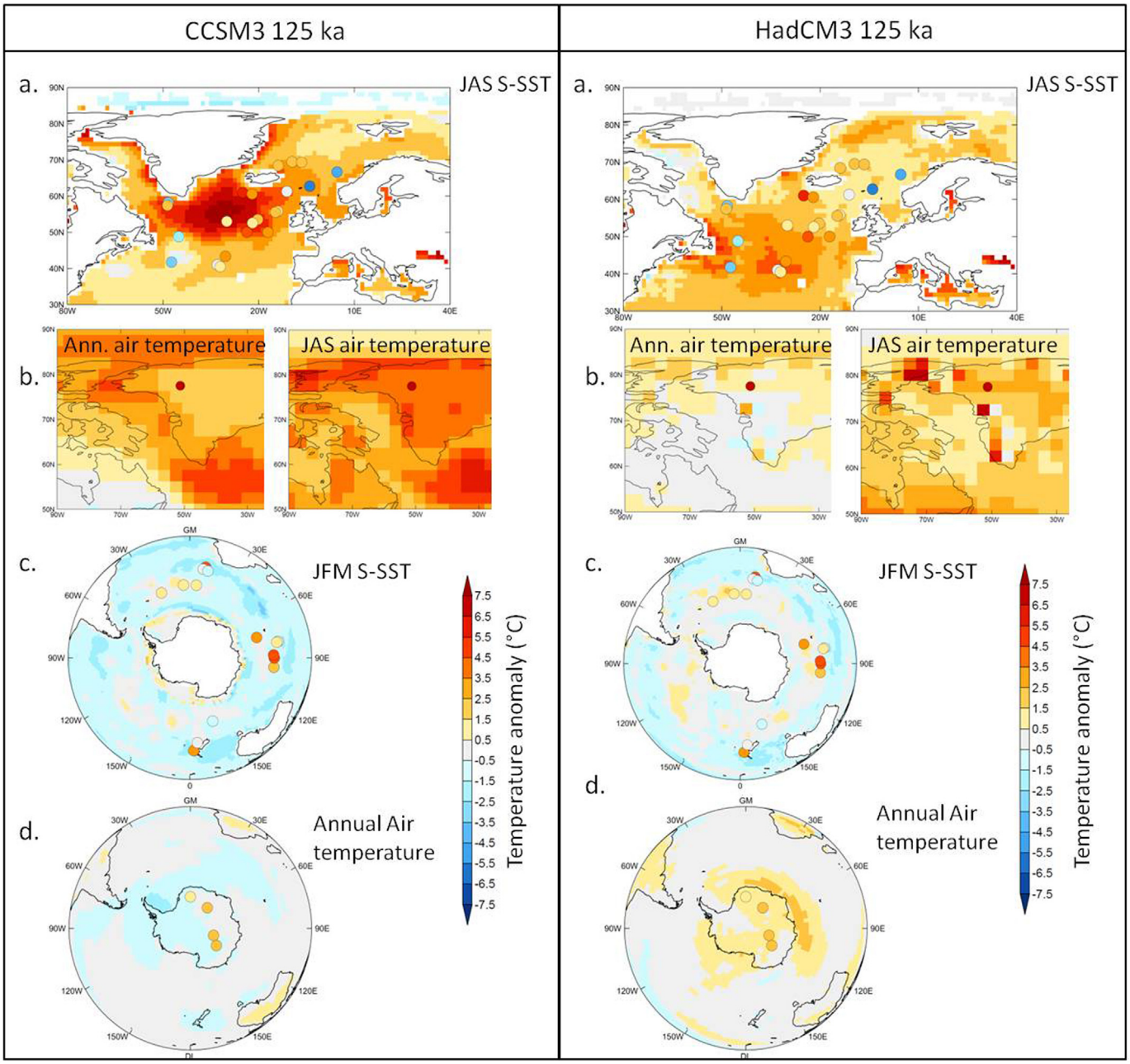

Fig. 7. 125 ka Model-data comparison for the time slice at 125 ka, using the (left panel) CCSM3 and (right panel) HadCM3 models. a. Summer SST temperature anomalies from the marine sediment data (dots) superimposed onto model July–August–September SST simulation in the Northern Hemisphere; b. Precipitation-weighed temperature anomaly reconstructed from the NEEM ice core (dot) superimposed onto precipitation-weighed temperature simulated above Greenland; c. Summer SST temperature anomalies from the marine sediment data (dots) superimposed onto the model January–February–March SST simulation in the Southern Ocean; d. Annual surface air temperature anomalies from the ice core data (dots) superimposed onto the model annual simulation.

conditions in the southern high latitudes. In other words, the linear response to summer insolation changes in the Northern Hemisphere and the lack of response to orbital forcing in the Southern Hemisphere are not consistent with air and sea surface temperature reconstructions.

In the Northern Hemisphere high latitudes, the CCSM3 125 ka simulation exhibits higher computed than reconstructed SST by up to 6 °C in specific locations (e.g. [16], [17] and [18]). It is in agreement within less than 2 °C with the reconstructed data records at some other locations (e.g. [22], [23], [25] and [26]). Considering the uncertainty range associated with SST estimates, HadCM3 results are generally in good agreement with Northern Hemisphere high latitudes SST data for 125 ka. However, both models fail at reproducing the reconstructed temperature anomalies at the sites characterised by cooler than present day sea surface conditions ([5], [6], [7], [21] and [24]). Note that the differences observed between the CCSM3 and HadCM3 simulations are likely related to their sea ice sensitivities with CCSM3 being more sensitive in the Northern Hemisphere and less sensitive in the Southern Hemisphere than HadCM3 (Otto-Bliesner et al., 2013).

Although they simulate warmer conditions over the Greenland ice sheet, neither of the 125 ka simulations are able to produce a warming as strong as that estimated from the NEEM ice core (7 ± 4 °C at 125 ka) in precipitation-weighted air

temperature (Fig. 7b). However, an uncertainty of ±4 °C is associated with the NEEM precipitation-weighted temperature anomaly. Furthermore, interpretation of Greenland water isotopic profiles in terms of temperature remains challenging due to the seasonality affecting the precipitations, changes in ice sheet topography (e.g. Vinther et al., 2009; NEEM c. m. 2013), and the possible effects of boundary conditions such as sea ice extent on the relationship between temperature and isotopic content (Sime et al., 2009).

In the Southern Ocean, data and simulations present fairly similar summer sea surface conditions at 125 ka compared to 130 ka given the associated temperature uncertainty. As for Antarctic surface air temperature, cooler than present day annual conditions are observed in the 125 ka CCSM3 simulation. The HadCM3 125 ka simulation shows warmer-than-present annual conditions in agreement within 2 °C with the climatic conditions depicted in ice core data. Note that for both models, simulations represent best the warmer-than-present-day conditions at the location of ice core data when considering winter air temperature over Antarctica (simulation data not shown). This seasonal aspect would deserve further investigations.

Fig. 8 represents the difference between the 125 ka and the 130 ka climatic conditions. It strengthens our observations about the climatic changes in the course of Termination II in the Northern Hemisphere. Indeed, it provides a model-data comparison free from the uncertainty associated with the choice of the reference temperature in both the models and the data for present day conditions (Section 2.4). This comparison highlights that the magnitude of Northern Hemisphere SST changes between 130 and 125 ka is not represented in both models simulations. The warming observed in the data is underestimated by up to 5 °C in the HadCM3 simulation while a slight cooling is produced in the CCSM3 simulation.

Both models correctly simulate the absence of significant climatic changes in the Southern Ocean between 130 and 125 ka. Finally, ice core data depict a stable or slightly colder climate (between 0 ± 1.5 °C and −1.5 ± 1.5 °C) that is reproduced in the CCSM3 [125 ka minus 130 ka] simulation while HadCM3 produces a slight warming (between 0.5 and 1.5 °C).

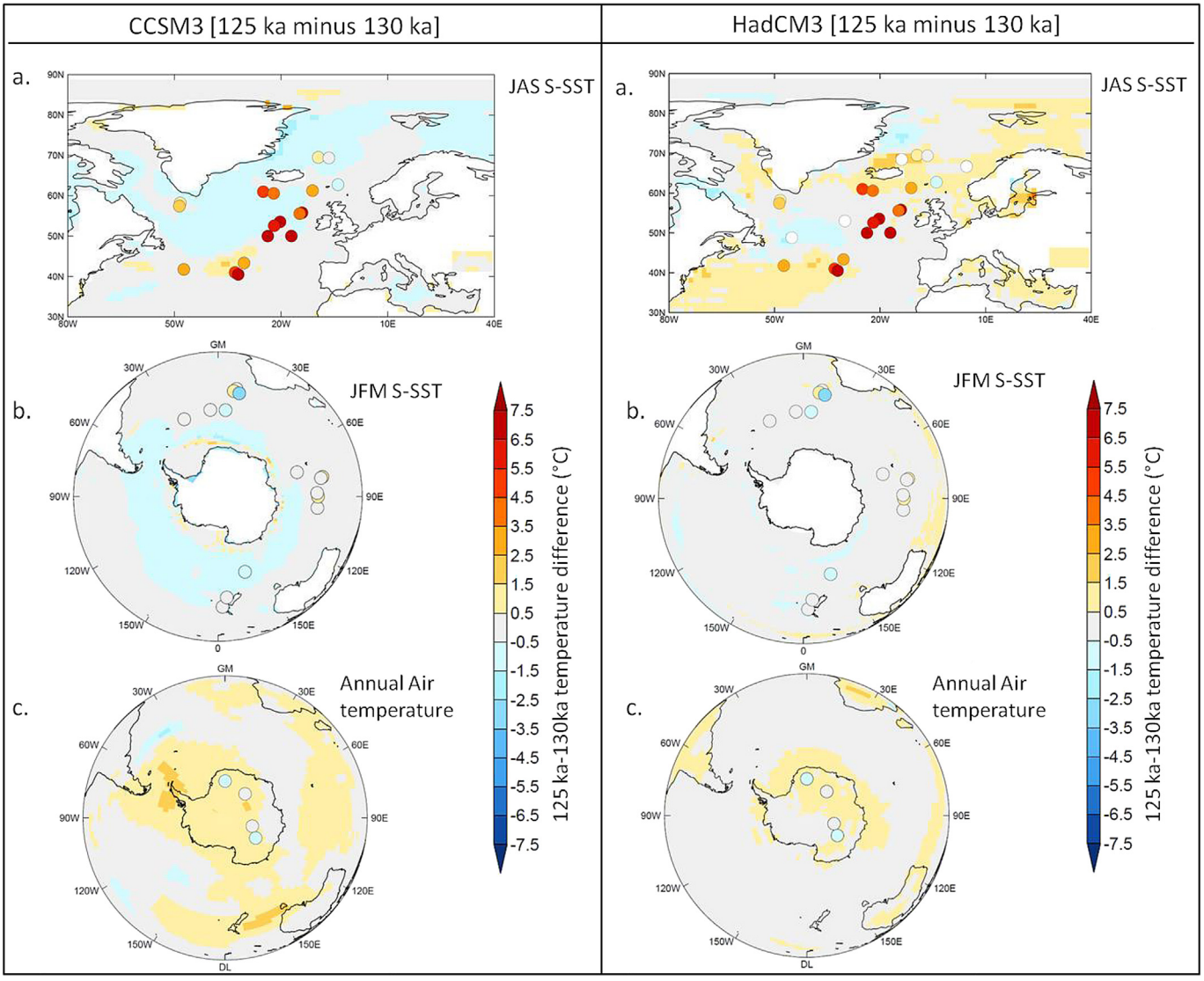

Fig. 8. Temperature difference between 125 ka climatic conditions and 130 ka climatic conditions both as recorded in Antarctic ice core and marine sediment data and as simulated by CCSM3 (left panel) and HadCM3 (right panel). In both models, simulated Summer SST are calculated as a temperature average over the months JFM and JAS for the a. Northern Hemisphere and b. the Southern Hemisphere Summer SST respectively. c. Simulated annual air temperatures are compared with air temperature anomalies inferred from Antarctic ice cores.

4. Discussion

4.1. Potential and limits of the new LIG spatio-temporal data synthesis

The SST records of our data synthesis have been derived from various methods. The MARGO SST synthesis for the Last Glacial Maximum time period shows that using different microfossil proxies yield discrepancies in SST estimates above 35°N (MARGO project members, 2009). Unfortunately, quantitatively assessing the temperature uncertainties related to the use of SST records based on different methods in our case is difficult since only two cores MD03-2664 and SU90-08 benefit from multiple SST reconstructions. For site SU90-08, the comparison of the MAT-based SST reconstruction ([23], Fig. 4) with the alkenone-based SST reconstruction [22] shows that major transitions are recorded at the same time but higher maximum LIG temperature and larger amplitude changes are observed in the MAT-based summer SST reconstruction compared to the alkenone-based SST reconstruction. However, alkenone-based SST is usually interpreted as reflecting annual conditions (Müller et al., 1998; Sachs et al., 2000), while MAT-based SST reflects summer conditions. SST reconstructions based both on the Mg/Ca ratio [13] and MAT [12] are available for core MD03-2664. Mg/Ca ratio-based temperatures are systematically lower than MAT-based summer SST but higher than MAT-based winter SST. Irvali et al. (2012) suggest that this pattern illustrates that the Mg/Ca ratio-based SST estimates might reflect spring conditions. As a result, SST signals from those two cores highlight the difficulty of comparing SST records from different proxies, because reconstructed SSTs may represent different seasonal or annual signals. Previous studies have already reported this issue and also highlight an additional bias derived from the different calibration datasets used in the SST reconstructions (e.g. de Vernal et al., 2006; Hessler et al., 2014). Overall, combining LIG SST reconstructions inferred from different methods may induce inconsistencies in the reconstructed SST records, creating difficulties when comparing absolute values. However, this issue is reduced in our case since SST estimates derived from faunal assemblages dominate (30 out of 42 records). Additional high-resolution SST records based on various proxy methods would be required to carefully assess quantitatively how much the use of various SST reconstruction methods influences the temporal LIG characteristics highlighted in this study.

Mean annual or summer SST for each marine core location were extracted at 10 m depth from the 1998 World Ocean Atlas (WOA98) to develop a comparison to modern time annual and summer SST. Core top SST reconstructions can diverge from the WOA98 SST (Table A1) and this may introduce systematic offsets in temperature anomaly calculations. Using only core top SST estimates based on the same proxy as LIG SST reconstructions is not possible because this top-core information is available in a few selected records only (Fig. A1). Using core top SST values as modern time references is also complicated by the perturbation or the loss of most recent sediments during coring procedure. When available, we compare the temperature anomaly obtained from core top SST and modern WOA SST as reference temperatures. Fig. A1 presents the data-based time slices with temperature anomalies calculated with the core-top SSTs as references. It illustrates that the major climatic features and patterns described on Fig. 5 are also visible when considering core top SST as present-day reference, i.e. an early Southern Hemisphere high-latitude warming compared to the Northern Hemisphere high-latitudes, longer warmer-than present conditions in the Southern Hemisphere and larger amplitude of temperature changes in the high Northern latitudes.

In addition, we are aware that considering summer (JAS SST in the Northern Hemisphere; JFM SST in the Southern Hemisphere) temperature at 10 m water-depth as modern reference might be a poor representation of the modern habitat of foraminiferal species in terms of season and water-depth (e.g. Tolderlund and Bé, 1971; Kohfeld et al., 1996; Simstich et al., 2003; Jonkers et al., 2010). However, we consider that it represents the most appropriate choice here to calculate past temperature anomalies, because it corresponds to the calibration depth and season that are included in the calibration core top database (e.g. Kucera et al., 2005; MARGO c. m. 2009) used in SST transfer functions to reconstruct past SST changes. Also, we highlight in the previous paragraph that we observe similar major climatic features and patterns when comparing temperature anomalies calculated vs WOA or core top values, which suggests that the choice of WOA modern values at 10 m water-depth has little effect on the main results of our study.

Estimated uncertainties are about 2.6 °C on average for marine sediment cores and set at 1.5 °C for Antarctic ice cores and 4 °C for the NEEM ice core. This means that they are frequently of the same amplitude as the calculated temperature anomaly itself. However, it is possible to highlight with confidence some climatic patterns in the Southern Hemisphere and the North Atlantic region based on observations made on multiple records. For instance, we consider that a warmer than present-day Southern Ocean by about +2 °C is a robust climatic feature on the 125 and 130 ka data-based time slices since it is observed in most of the considered marine records even though taken individually each SST anomaly is associated with an error of similar magnitude.

Although we are confident in the age models developed for the Southern Ocean and North Atlantic marine records, one should keep in mind that defining robust and coherent chronologies for SST records from the Nordic Seas remains difficult and that the associated relative uncertainty is large (~3–4 ka). This feature results from the current limitations associated with SST reconstruction method based on the percentage of the polar species *N. pachyderma* sinistral, and the difficulty to identify unambiguously stratigraphic markers between cores. Consequently, it is difficult to identify robust climatic patterns in this region. Future high-resolution SST records based on alternative proxies and the identification of new stratigraphic markers (e.g. tephra horizons, Davies et al., 2014) should help to improve chronologies for palaeoclimatic records from in this region.

While previous compilations already demonstrated warmer-than-present-day conditions prevailing during the LIG, the emphasis of these compilations was on quantifying the maximum in temperature warmth rather than on the temporal evolution of the climatic conditions across the time-period. The data synthesis of Turney and Jones (2010) reported the early Antarctic warming but their work was lacking a common temporal framework between climatic records. Our work is the first LIG compilation associated with a common time frame between marine and ice high-latitude records from both hemispheres. This enables to provide a detailed spatio-temporal information on the evolution of high-latitude temperature throughout the LIG. We also propagate age uncertainties and include SST reconstruction method errors in order to map for the first time high latitude temperature anomalies for four time slices covering the LIG.

4.2. GCM snapshot simulations vs data-based time slices: mismatch and implications

Otto-Bliesner et al. (2013) used the LIG compilations from Turney and Jones (2010) and McKay et al. (2011) to benchmark two CCSM3 snapshot simulations performed under 125 and 130 ka conditions for the orbital and greenhouse gas concentration

forcing. However, they could not perform a detailed evaluation of the model simulations for each considered time period since both compilations present only peak warmth information. Now, we are able to investigate in particular, the capability of two GCMs in reproducing asynchronous climate variations at the beginning of the LIG in polar and sub-polar regions. The warming in the Southern Ocean and over Antarctica occurred prior to peak warmth in the North Atlantic, Nordic Seas, and Greenland at the beginning of the LIG (Masson-Delmotte et al., 2010; Bauch et al., 2011; Govin et al., 2012; NEEM c. m., 2013). This delay in peak warmth conditions between the northern and southern high latitudes illustrated on the 130 ka time slice is attributed to the "bipolar seesaw" mechanism induced by changes in the intensity of the Atlantic Meridional Overturning Circulation (AMOC; Stocker and Johnsen, 2003; Masson-Delmotte et al., 2010; Holden et al., 2010). The melting of northern ice sheets during Termination II into the early LIG has been suggested to delay the full establishment of a vigorous AMOC, which coincides with peak Antarctic temperature (Govin et al., 2012).

The HadCM3 and CCSM3 simulations do not reproduce such a bipolar seesaw pattern since they only simulate the climate response to the LIG orbital and greenhouse forcing (Table A3), without taking into account physical processes which can redistribute heat from the north to the south, in particular through the impact of ice sheet freshwater on the AMOC, absent from these particular simulations. Simulations introducing freshwater forcing to account for a bipolar seesaw response to persistent iceberg melting at northern high latitudes (Govin et al., 2012) and disintegration of the WAIS (Langebroek and Nisancioglu, 2014) better reproduce the late LIG Northern Hemisphere warming (Holden et al., 2010). A recent modelling study focused on the last deglaciation (Ritz et al., 2013) showed that inclusion of the Northern Hemisphere remnant ice sheets resulted in a delay in warming at high Northern Hemisphere latitudes by ~2000 years compared with modelling studies which only included the modern ice sheets (Bakker et al., 2013). In addition, the Ritz et al. (2013) study included freshwater forcing from the melting ice responding to the enhanced warming.

Moreover, the mismatches in term of both the sign and the amplitude in temperature changes are likely to originate from the fact that not all appropriate changes in the boundary conditions have been considered in the design of the experiments. In particular, both models include present-day vegetation and polar ice sheet distribution. Previous modelling of the LIG has shown that feedbacks between vegetation and climate enhance the warming at high latitudes (Crucifix and Loutre, 2002; Schurgers et al., 2007). Otto-Bliesner et al. (2013) present also a sensitivity simulation with CCSM3 with the removal of the WAIS. It provides additional local warming over Antarctica but still not enough to explain the ice core records. Simulations with HadCM3 by Holden et al. (2010) suggest that in addition to the WAIS retreat, freshwater input to the North Atlantic from the Laurentide and Eurasian ice sheets during Termination II is required to agree with the warming indicated by Antarctic ice core records. Differences between model simulations presented in this paper and data may also be related to model representations of atmospheric feedbacks (e.g. liquid water in Arctic clouds) and missing feedbacks linked to sea ice and snow cover processes (e.g. rain and snow melt albedo), and prescribed changes in ice sheet topography (e.g. Masson-Delmotte et al., 2006; Born et al., 2010; Fischer and Jungclaus, 2010; Masson-Delmotte et al., 2011a; Otto-Bliesner et al., 2013).

Our results illustrate that during the LIG, as-warm or warmer conditions than today have prevailed for a longer time period in the Southern Hemisphere than in the Northern Hemisphere (Fig. 5). Larger amplitude temperature changes are also recorded over the polar ice sheet than in the surrounding surface ocean. This is particularly obvious in the amplitude changes over Termination II and over the glacial inception (Fig. 4). Such a difference originates (i) from the fact that land areas on average change more rapidly than the ocean (land–sea contrast; e.g. Joshi et al., 2008; Braconnot et al., 2012) and (ii) from the polar amplification due to feedbacks related to surface albedo (land ice and sea ice cover), ice sheet elevation and atmospheric processes (e.g. Holland and Bitz, 2003; Masson-Delmotte et al., 2006).

5. Concluding remarks

We have selected 47 air and sea surface temperature records from ice and marine sediment cores with a temporal resolution of at least 2000 years covering the LIG. All records have been aligned onto the most recent AICC2012 ice core chronology and this enables investigation into the temporal evolution of the climate over the LIG in polar and sub-polar regions. This is the first synthesis over the LIG associated with consistent chronologies and a careful consideration of dating uncertainties. The major features highlighted are (i) non synchronous maximum temperature changes between the two hemispheres with the Southern Ocean and Antarctica records showing an early warming compared to Northern Hemisphere high latitude records, (ii) warmer than present-day conditions exhibited in Southern Hemisphere records for a longer time period compared to records from the Northern Hemisphere, and (iii) larger amplitude of temperature changes at high northern latitudes compared to high southern latitudes recorded at the onset and the demise of the LIG.

We provide for the first time a spatial and temporal evolution of the LIG climate rather than a snapshot vision on the climatic optimum in the high latitudes of both hemispheres. It allows more precise model-data comparison over the LIG. For this purpose, we have produced four data-based time slices at 115, 120, 125 and 130 ka of the temperature anomalies compared to modern conditions, associated with quantitatively estimated temperature uncertainties including dating errors. We have compared CCSM3 and HadCM3 surface temperature model simulations for 130 and 125 ka to the respective 130 and 125 ka data time slices. Our comparison shows that the models predict warmer than present conditions earlier than documented in the Northern Hemisphere high latitude region, while the reconstructed early Southern Ocean and Antarctic warming is not captured by any model. Our results highlight the importance of producing time slices rather than one representative climate for the LIG. They also provide additional evidence that missing processes (ice sheet melt and associated freshwater fluxes, vegetation feedbacks) likely result in the inability of CCM3 and HadCM3 to capture the temporal signal observed in the data (Otto-Bliesner et al., 2013). This limits identification of potential parametric or structural errors in the processes that are taken into account in climate models (e.g. sea ice, polar clouds, snow albedo).

Hopefully, this work will encourage more in-depth data-model comparison exercises with both snapshots (e.g. Lunt et al., 2013) and transient (e.g. Bakker et al., 2013; Langebroek and Nisancioglu, 2014) climate model simulations that will also involve rigorous statistical analysis.

Here, we have focused on air and sea surface temperature. However, future work should also focused on additional information provided by the selected and future new records (e.g. changes in AMOC intensity, sea ice extent) to move towards a more complete picture of environmental changes during the LIG. Finally, improved model-data comparison techniques such as the use of models which explicitly simulate climate proxies (e.g. ice $\delta^{18}O$, benthic and/or planktic $\delta^{18}O$, planktic foraminifera assemblage; Telford et al., 2013) would allow more effective use of the

paleoclimate information by facilitating a direct comparison between model and proxy.

Acknowledgements

We thank Elsa Cortijo for sharing unpublished SST records, Elisabeth Michel for participating to the initial marine record synthesis effort and Chronis Tzedakis for helpful discussions. E. Thomsen (Aarhus University, Denmark) is thanked for the running of transfer functions based on the 100 μm planktic data of core ENAM33.

We are very grateful to two anonymous reviewers and Henning Bauch for their constructive comments that help improving this manuscript. A. Govin was supported by the Deutsche Forschungsgemeinschaft (DFG) under the Special Priority Programme INTERDYNAMIC (EndLIG project, grant GO 2122/1-1). The research leading to these results has received funding from the UK-NERC consortium iGlass (NE/I009906/1) and is also a contribution to the European Union's Seventh Framework programme (FP7/2007–2013) under grant agreement 243908, "Past4Future. Climate change – Learning from the past climate". This is Past4Future contribution no 79.

Appendix A. Supplementary data

Supplementary data related to this article can be found at http://dx.doi.org/10.1016/j.quascirev.2014.08.018.

References

Bakker, P., Masson-Delmotte, V., Martrat, B., Charbit, S., Renssen, H., Gröger, M., Krebs-Kanzow, U., Lohman, G., Lunt, D.J., Pfeiffer, M., Phipps, S.J., Prange, M., Ritz, S.P., Schulz, M., Stenni, B., Stone, E.J., Varma, V., 2014. Temperature trends during the Present and Last interglacial periods - a multi-model-data comparison. Quat. Sci. Rev. 99, 224–243.

Bakker, P., Stone, E.J., Charbit, S., Chroger, M., Krebs-Kanzow, U., Ritz, S.P., Varma, V., Khon, V., Lunt, D.J., Mikolajewicz, U., Prange, M., Renssen, H., Schneider, B., Schulz, M., 2013. Last interglacial temperature evolution - a model inter-comparison. Clim. Past 9, 605–619.

Bauch, H.A., Erlenkeuser, H., 2008. A "critical" climatic evaluation of last interglacial (MIS 5e) records from the Norwegian Sea. Polar Res. 27, 135–151.

Bauch, H.A., Erlenkeuser, H., Jung, S.J.A., Thiede, J., 2000. surface and deep water changes in the subpolar North Atlantic during Termination II and the Last Interglaciation. Paleoceanography 15, 76–84.

Bauch, D., Bauch, H.A., 2001. Last glacial benthic foraminiferal δ18O anomalies in the polar North Atlantic: A modern analogue evaluation. Journal of Geophysical Research: Oceans 106, 9135–9143. http://dx.doi.org/9110.1029/1999jc000164.

Bauch, H.A., Kandiano, E.S., Helmke, J., Andersen, N., Rosell-Mele, A., Erlenkeuser, H., 2011. Climatic bisection of the last interglacial warm period in the Polar North Atlantic. Quat. Sci. Rev. 30, 1813–1818 doi:1810.1016/j.quascirev.2011.1805.1012.

Bauch, H.A., Kandiano, E.S., Helmke, J.P., 2012. Contrasting ocean changes between the subpolar and polar North Atlantic during the past 135 ka. Geophys. Res. Lett. 39 http://dx.doi.org/10.1029/2012GL051800.

Baumgartner, M., Kindler, P., Eicher, O., Floch, G., Schilt, A., Schwander, J., Spahni, R., Capron, E., Chappellaz, J., Leuenberger, M., Fischer, H., Stocker, T.F., 2013. NGRIP CH_4 concentration from 120 to 10 kyr before present and its relation to a $\delta^{15}N$ temperature reconstruction from the same ice core. Clim. Past Discuss. 9, 4655–4704.

Bazin, L., Landais, A., Lemieux-Dudon, B., Toyé Mahamadou Kele, H., Veres, D., Parrenin, F., Martinerie, P., Ritz, C., Capron, E., Lipenkov, V., Loutre, M.-F., Raynaud, D., Vinther, B., Svensson, A., Rasmussen, S.O., Severi, M., Blunier, T., Leuenberger, M., Fischer, H., Masson-Delmotte, V., Chappellaz, J., Wolff, E.W., 2013. An optimized multi-proxy, multi-site Antarctic ice and gas orbital chronology (AICC2012): 120–800 ka. Clim. Past 9, 1715–1731.

Birks, H.J.B., 1998. Numerical tools in palaeolimnology - progress, potentialities, and problems. J. Paleolimnol. 20, 307–332.

Bond, G.C., Broecker, W., Johnsen, S., McManus, J., Labeyrie, L., Jouzel, J., Bonani, G., 1993. Correlations between climate records from the North Atlantic sediments and Greenland Ice. Nature 365, 143–147.

Born, A., Nisancioglu, K.H., 2012. Melting of Northern Greenland during the last interglaciation. Cryosphere 6, 1239–1250.

Born, A., Nisancioglu, K.H., Braconnot, P., 2010. Sea ice induced changes in ocean circulation during the Eemian. Clim. Dyn. 35 (7–8), 1361–1371.

Braconnot, P., Harrison, S.P., Kageyama, M., Bartlein, P.J., Masson-Delmotte, V., Abe-Ouchi, A., Otto-Bliesner, B., Zhao, Y., 2012. Evaluation of climate models using palaeoclimatic data. Nat. Clim. Change. http://dx.doi.org/10.1038/NCLIMATE1456.

Bradley, S.L., Siddall, M., Milne, G.A., Masson-Delmotte, V., Wolff, E., 2012. Where might we find evidence of a Last Interglacial West Antarctic Ice Sheet collapse in Antarctic ice core records? Glob. Planet. Change 88–89, 64–75.

Bradley, S.L., Siddall, M., Milne, G.A., Masson-Delmotte, V., Wolff, E., 2013. Combining ice core records and ice sheet models to explore the evolution of the East Antarctic Ice sheet during the Last Interglacial period. Glob. Planet. Change 100, 278–290.

Calvo, E., Pelejero, C., de Deckker, P., Logan, G.A., 2007. Antarctic deglacial pattern in a 30 kyr record of sea surface temperature offshore South Australia. Geophys. Res. Lett. 34, L13707 doi:13710.11029/12007GL029937.

CAPE Last Interglacial Project Members, 2006. Last Interglacial Arctic warmth confirms polar amplification of climate change. Quat. Sci. Rev. 25, 1383–1400.

Chappellaz, J., Blunier, T., Raynaud, D., Barnola, J.-M., Schwander, J., Stauffer, B., 1993. Synchronous changes in atmospheric CH_4 and Greenland climate between 40 kyr and 8 kyr BP. Nature 366, 443–445.

Church, J.A., Clark, P.U., Cazenave, A., Gregory, J.M., Jevrejeva, S., Levermann, A., Merrifield, M.A., Milne, G.A., Nerem, R.S., Nunn, P.D., Payne, A.J., Pfeffer, W.T., Stammer, D., Unnikrishnan, A.S., 2013. Sea level change. In: Stocker, T.F., Qin, D., Plattner, G.-K., Tignor, M., Allen, S.K., Boschung, J., Nauels, A., Xia, Y., Bex, V., Midgley, P.M. (Eds.), Climate Change 2013: the Physical Science Basis. Contribution of Working Group I to the Fifth Assessment Report of the Intergovernmental Panel on Climate Change. Cambridge University Press, Cambridge, United Kingdom and New York, NY, USA.

Clark, P.U., Huybers, P., 2009. Interglacial and future sea level. Nature 462, 856–857.

CLIMAP, 1984. The last interglacial ocean. Quat. Res. 21, 123–224.

Collins, W.D., Bitz, C.M., Blackmon, M.L., Bonan, G.B., Bretherton, C.S., Carton, J.A., Chang, P., Doney, S.C., Hack, J.J., Henderson, T.B., Kiehl, J.T., Large, W.G., McKenna, D.S., Santer, B.D., Smith, R.D., 2006. The community climate system model version 3 (CCSM3). J. Clim. 19, 2122–2143.

Cortijo, E., 1995. La variabilite climatique rapide dans l'Atlantique Nord depuis 128 000 ans: Relations entre les calottes de glace et l'ocean de surface (Ph.D. thesis). Univ. Paris XI, Orsay, France.

Cortijo, E., Lehman, S.J., Keigwin, L.D., Chapman, M.R., Paillard, D., Labeyrie, L., 1999. Changes in meridional temperature and salinity gradients in the North Atlantic Ocean (30°-72°N) during the last interglacial period. Paleoceanography 14, 22–33.

Crucifix, M., Loutre, M.F., 2002. Transient simulations over the last interglacial period (126-115 kyr BP): feedback and forcing analysis. Clim. Dyn. 19, 419–433.

Davies, S.M., Abbott, P.M., Meara, R.H., Pearce, N.J., Austin, W.E.N., Chapman, M., Svensson, A.M., Bigler, M., Rasmussen, T.L., Rasmussen, S.O., Farmer, E.J., 2014. A North Atlantic tephrostratigraphical framework for 130-60 ka b2k: new tephra discoveries, marine-based-correlations and future challenges. Quat. Sci. Rev. ISSN: 0277-3791 (2014). http://dx.doi.org/0210.1016/j.quascirev.2014.0203.0024.

de Vernal, A., Rosell-Mele, A., Kucera, M., Hillaire-Marcel, C., Eynaud, F., Weinelt, E., Dokken, T., Kageyama, M., 2006. Comparing proxies for the reconstruction of LGM sea-surface conditions in the northern North Atlantic. Quat. Sci. Rev. 25, 2820–2834.

Fischer, N., Jungclaus, J.H., 2010. Effects of orbital forcing on atmosphere and ocean heat transports in Holocene and Eemian climate simulations with a comprehensive earth system model. Clim. Past 6, 155–168 doi:110.5194/cp-5196-5155-2010.

Fronval, T., Jansen, E., Haflidason, H., Sejrup, H.-P., 1998. Variability in surface and deep water conditions in the Nordic seas during the last interglacial period. Quat. Sci. Rev. 17, 963–985.

Gordon, C., Cooper, C., Senior, C.A., Banks, H., Gregory, J.M., Johns, T.C., Mitchell, J.F.B., Wood, R.A., 2000. The simulation of SST, sea ice extents and ocean heat transports in a version of the Hadley Centre coupled model without flux adjustments. Clim. Dyn. 16, 147–168.

Govin, A., Braconnot, P., Capron, E., Cortijo, E., Duplessy, J.-C., Jansen, E., Labeyrie, L., 2012. Persistent influence of ice sheet melting on high northern latitude climate during the early Last Interglacial. Clim. Past 8, 483–507 doi:410.5194/cp-5198-5483-2012.

GRIP-members, 1993. Climate instability during the last interglacial period recorded in the GRIP ice core. Nature 364, 203–208.

Grootes, P.M., Stuiver, M., White, J.W.C., Johnsen, S.J., Jouzel, J., 1993. Comparison of the oxygen isotope records from the GISP2 and GRIP Greenland ice cores. Nature 366, 552–554.

Hessler, I., Harrison, S.P., Kucera, M., Waelbroeck, C., Chen, M.-T., Andersson, C., de Vernal, A., Fréchette, B., Cloke-Hayes, A., Leduc, G., Londeix, L., 2014. Implication of methodological uncertainties for Mid-Holocene sea surface temperature reconstructions. Clim. Past Discuss. 10, 1747–1782.

Holden, P.B., Edwards, N.R., Wolff, E.W., Lang, N.J., Singarayer, J.S., Valdes, P.J., Stocker, T.F., 2010. Interhemispheric coupling, the West Antarctic Ice Sheet and warm Antarctic interglacials. Clim. Past 6, 431–443.

Holland, M.M., Bitz, C.M., 2003. Polar amplification of climate change in coupled models. Climate Dynamics 21, 221–232.

Huber, C., Leuenberger, M., Spahni, R., Flückiger, J., Schwander, J., Stocker, T.F., Johnsen, S., Landais, A., Jouzel, J., 2006. Isotope calibrated Greenland temperature record over Marine Isotope Stage 3 and its relation to CH_4. Earth Planet. Sci. Lett. 243, 504–519.

Husum, K., Hald, M., 2012. Arctic planktic foraminiferal assemblages: implications for subsurface temperature reconstructions. Mar. Micropaleontol. 96–97, 38–47.

Irvali, N., Ninnemann, U.S., Galaasen, E.V., Rosenthal, Y., Kroon, D., Oppo, D.W., Kleiven, H.F., Darling, K.F., Kissel, C., 2012. Rapid switches in subpolar North Atlantic hydrography and climate during the Last Interglacial (MIS 5e). Paleoceanography 27, PA220 doi:210.1029/2011PA002244.

Jonkers, L., Brummer, G.-J.A., Peeters, F.J.C., van Aken, H.M., De Jong, M.F., 2010. Seasonal stratification, shell flux, and oxygen isotope dynamics of left-coiling *N. pachyderma* and *T. quinqueloba* in the western subpolar North Atlantic. Paleoceanography 25, PA2204.

Joshi, M.M., Gregory, J.M., Webb, M.J., Sexton, D.M.H., Johns, T.C., 2008. Mechanisms for the land/sea warming contrast exhibited by simulations of climate change. Clim. Dyn. 30, 455–465.

Jouzel, J., Masson-Delmotte, V., Cattani, O., Dreyfus, G., Falourd, S., Hoffmann, G., Minster, B., Nouet, J., Barnola, J.-M., Fisher, H., Gallet, J.-C., Johnsen, S., Leuenberger, M., Loulergue, L., Luethi, D., Oerter, H., Parrenin, F., Raisbeck, G., Raynaud, D., Schilt, A., Schwander, J., Selmo, J., Souchez, R., Spahni, R., Stauffer, B., Steffensen, J.P., Stenni, B., Stocker, T.F., Tison, J.-L., Werner, M., Wolff, E.W., 2007. Orbital and millennial Antarctic climate variability over the past 800,000 years. Science 317, 793–796.

Jouzel, J., Vimeux, F., Caillon, N., Delaygue, G., Hoffmann, G., Masson-Delmotte, V., Parrenin, F., 2003. Magnitude of the isotope/temperature scaling for interpretation of central Antarctic ice cores. J. Geophys. Res. 108, 1029–1046.

Juggins, S., 2007. C2 Version 1.5 User Guide. Software for Ecological and Palaeoecological Data Analysis and Visualisation. Newcastle University, Newcastle upon Tyne, UK.

Kaspar, F., Kuhl, N., Cubasch, U., Litt, T., 2005. A model-data comparison of European temperatures in the Eemian interglacial. Geophys. Res. Lett. http://dx.doi.org/10.1029/2005GL022456.

Kohfeld, K.E., Fairbanks, R.G., Smith, S.L., Walsh, I.D., 1996. *Neogloboquadrina pachyderma* (sinistral coiling) as paleoceanographic tracers in polar oceans: evidence from northeast water polynya plankton tows, sediment traps, and surface sediments. Paleoceanography 11, 679–699, 610.1029/1096pa02617.

Kopp, R.E., Simons, F.J., Mitrovica, J.X., Maloof, A.C., Oppenheimer, M., 2009. Probabilistic assessment of sea level during the last interglacial stage. Nature 462, 863–867 doi:810.1038/nature08686.

Kucera, M., Rosell-Melé, A., Schneider, R., Waelbroeck, C., Weinelt, M., 2005. Multiproxy approach for the reconstruction of the glacial ocean surface (MARGO). Quat. Sci. Rev. 24, 813–819.

Langebroek, P.M., Nisancioglu, K.H., 2014. Simulating last interglacial climate with NorESM: role of insolation and greenhouse gases in the timing of peak warmth. Clim. Past 10, 1305–1318.

Laskar, J., Robutel, P., Joutel, F., Gastineau, M., Correia, A.C.M., Levrard, B., 2004. A long-term numerical solution for the insolation quantities of the Earth. Astron. Astrophys. 428, 261–285.

Lisiecki, L.E., Raymo, M.E., 2005. Plio-Pleistocene stack of 57 globally distributed benthic d^{18}O records. Paleoceanography 20. http://dx.doi.org/10.1029/2004PA001071.

Lisiecki, L.E., Raymo, M.E., 2009. Diachronous benthic d18O responses during late Pleistocene terminations. Paleoceanography 24, PA3210. http://dx.doi.org/10.1029/2009PA001732.

Locarnini, R.A., Mishonov, A.V., Antonov, J.I., Boyer, T.P., Garcia, H.E., Baranova, O.K., Zweng, M.M., Johnson, D.R., 2010. World ocean atlas 2009, volume 1: temperature. In: Levitus, S. (Ed.), NOAA Atlas NESDIS 68. U.S. Government Printing Office, Washington, D.C., 184 pp.

Loulergue, L., Schilt, A., Spahni, R., Masson-Delmotte, V., Blunier, T., Lemieux, B., Barnola, J.M., Raynaud, D., Stocker, T.F., Chappellaz, J., 2008. Orbital and millennial-scale features of atmospheric CH_4 over the past 800,000 years. Nature 453, 383–386.

Lunt, D.J., Abe-Ouchi, A., Bakker, P., Berger, A., Braconnot, P., Charbit, S., Fischer, N., Herold, N., Jungclaus, J.H., Khon, V.C., Krebs-Kanzow, U., Langebroek, P.M., Lohmann, G., Nisancioglu, K.H., Otto-Bliesner, B.L., Park, W., Pfeiffer, M., Phipps, S.J., Prange, M., Rachmayani, R., Renssen, H., Rosenbloom, N., Schneider, B., Stone, E.J., Takahashi, E., Wei, W., Yin, Q., Zang, Z.S., 2013. A multi-model assessment of last interglacial temperatures. Clim. Past 9, 699–717.

Lüthi, D., Le Floch, M., Bereiter, B., Blunier, T., Barnola, J.-M., Siegenthaler, U., Raynaud, D., Jouzel, J., Fischer, H., Kawamura, K., Stocker, T.F., 2008. High-resolution carbon dioxide concentration record 650,000-800,000 years before present. Nature 453, 379–382.

MARGO project members, 2009. Constraints on the magnitude and patterns of ocean cooling at the Last Glacial Maximum. Nature Geosciences 2, 127–132.

Martrat, B., Jimenez-Amat, P., Zahn, R., Grimalt, J.O., 2014. Similarities and dissimilarities between the last two deglaciations and interglaciations in the North Atlantic region. Quat. Sci. Rev. 99, 122–134.

Masson-Delmotte, V., Braconnot, P., Hoffmann, G., Jouzel, J., Kageyama, M., Landais, A., Lejeune, Q., Risi, C., Sime, L., Sjolte, J., Swingedouw, D., Vinther, B., 2011a. Sensitivity of interglacial Greenland temperature and δ18O: ice core data, orbital and increased CO2 climate simulations. Clim. Past 7, 1041–1059 doi:1010.5194/cp-1047-1041-2011.

Masson-Delmotte, V., Buiron, D., Ekaykin, A., Frezzotti, M., Gallée, H., Jouzel, J., Krinner, G., Landais, A., Motoyama, H., Oerter, H., Pol, K., Pollard, D., Ritz, C., Schlosser, E., Sime, L.C., Sodemann, L., Stenni, B., Uemura, R., Vimeux, F., 2011b. A comparison of the present and last interglacial periods in six Antarctic ice cores. Clim. Past 7, 397–423.

Masson-Delmotte, V., Kageyama, M., Braconnot, P., Charbit, S., Krinner, G., Ritz, C., Guilyardi, E., Jouzel, J., Abe-Ouchi, A., Crucifix, M., Gladstone, R.M., Hewitt, C.D., Kitoh, A., Legrande, A., Marti, O., Merkel, U., Motoi, T., Ohgaito, R., Otto-Bliesner, B., Peltier, W.R., Ross, I., Valdes, P.J., Vettoretti, G., Weber, S.L., Wolk, F., 2006. Past and future polar amplification of climate change: climate model intercomparisons and ice-core constraints. Clim. Dyn. ISSN: 0930-7575.

Masson-Delmotte, V., Schulz, M., Abe-Ouchi, A., Beer, J., Ganopolski, A., González Rouco, J.F., Jansen, E., Lambeck, K., Luterbacher, J., Naish, T., Osborn, T., Otto-Bliesner, B., Quinn, T., Ramesh, R., Rojas, M., Shao, X., Timmermann, A., 2013. Information from paleoclimate archives. In: Stocker, T.F., Qin, D., Plattner, G.-K., Tignor, M., Allen, S.K., Boschung, J., Nauels, A., Xia, Y., Bex, V., Midgley, P.M. (Eds.), Climate Change 2013: the Physical Science Basis. Contribution of Working Group I to the Fifth Assessment Report of the Intergovernmental Panel on Climate Change. Cambridge University Press, Cambridge, United Kingdom and New York, NY, USA.

Masson-Delmotte, V., Stenni, B., Blunier, T., Cattani, O., Chappellaz, J., Cheng, H., Dreyfus, G., Edwards, R.L., Falourd, S., Govin, A., Kawamura, K., Johnsen, S.J., Jouzel, J., Landais, A., Lemieux-Dudon, B., Lourantou, A., Marshall, G., Minster, B., Mudelsee, M., Pol, K., Röthlisberger, R., Selmo, E., Waelbroeck, C., 2010. Abrupt change of Antarctic moisture origin at the end of Termination II. Proc. Natl. Acad. Sci. http://dx.doi.org/10.1073/pnas.0914536107.

McKay, N.P., Overpeck, J.T., Otto-Bliesner, B.L., 2011. The role of ocean thermal expansion in Last Interglacial sea level rise. Geophys. Res. Lett. 38 http://dx.doi.org/10.1029/2011GL048280.

Müller, P.J., Kirst, G., Ruhland, G., von Storch, I., Rosell-Melé, A., 1998. Calibration of the alkenone paleotemperature index U37K′ based on core-tops from the eastern South Atlantic and the global ocean (60°N-60°S). Geochim. Cosmochim. Acta 62, 1757–1772.

NEEM-community-members, 2013. Eemian interglacial reconstructed from a Greenland folded ice core. Nature 493, 489–493 doi:410.1038/nature11789.

Nikolova, I., Yin, Q., Berger, A., Singh, U.K., Karami, M.P., 2013. The last interglacial (Eemian) climate simulated by LOVECLIM and CCSM3. Clim. Past 9, 1789–1806.

NorthGRIP-community-members, 2004. High-resolution record of Northern Hemisphere climate extending into the last interglacial period. Nature 431, 147–151.

Otto-Bliesner, B., Rosenbloom, N., Stone, E., McKay, N.P., Lunt, D.J., Brady, E.C., Overpeck, J.T., 2013. How warm was the Last Interglacial? New model-data comparisons. Philos. Trans. R. Soc. A Phys. Math. Eng. Sci. http://dx.doi.org/10.1098/rsta.2013.0097.

Paillard, D., Labeyrie, L., Yiou, P., 1996. Macintosh program performs time-series analyses. Eos Trans. Am. Geophys. Union 77 (39), 379.

Parrenin, F., Barnola, J.M., Beer, J., Blunier, T., Castellano, E., Chappellaz, J., Dreyfus, G., Fischer, H., Fujita, S., Jouzel, J., Kawamura, K., Lemieux-Dudon, B., Loulergue, L., Masson-Delmotte, V., Narcisi, B., Petit, J.R., Raisbeck, G., Raynaud, D., Ruth, U., Schwander, J., Severi, M., Spahni, R., Steffensen, J.P., Svensson, A., Udisti, R., Waelbroeck, C., Wolff, E., 2007. The EDC3 chronology for the EPICA Dome C ice core. Clim. Past 3, 485–497.

Quiquet, A., Ritz, C., Punge, H.J., Salas y Mélia, D., 2013. Greenland ice sheet contribution to sea level rise during the last interglacial period: a modelling study driven and constrained by ice core data. Clim. Past 9, 353–366.

Rasmussen, T.L., Bäckström, D., Heinemeier, J., Klitgaard-Kristensen, D., Knutz, P.C., Kuijpers, A., Lassen, S., Thomsen, E., Troelstra, S.R., van Weering, T.C.E., 2002. The Faeroe-Shetland Gateway: Late Quaternary water mass exchange between the Nordic seas and the northeastern Atlantic. Mar. Geol. 188, 165–192.

Rasmussen, T.L., Thomsen, E., Kuijpers, A., Wastegard, S., 2003. Late warming and early cooling of the sea surface in the Nordic seas during MIS 5e (Eemian Interglacial). Quat. Sci. Rev. 22, 809–821.

Rayner, N.A., Parker, D.E., Horton, E.B., Folland, C.K., Alexander, L.V., Rowell, D.P., Kent, E.C., Kaplan, A., 2003. Global analyses of sea surface temperature, sea ice, and night marine air temperature since the late nineteenth century. J. Geophys. Res. 108, 4407 doi:4410.1029/2002JD002670.

Risebrobakken, B., Balbon, E., Dokken, T., Jansen, E., Kissel, C., Labeyrie, L., Richter, T., Senneset, L., 2006. The penultimate deglaciation: high-resolution paleoceanographic evidence from a north-south transect along the eastern Nordic Seas. Earth Planet. Sci. Lett. 241, 505–516.

Ritz, S.P., Stocker, T.F., Grimalt, J.O., Menviel, L., Timmermann, A., 2013. Estimated strength of the Atlantic overturning circulation during the last deglaciation. Nat. Geosci. 6 http://dx.doi.org/10.1038/NGEO1723.

Robinson, A., Calov, R., Ganopolski, A., 2011. Greenland ice sheet model parameters constrained using simulations of the Eemian Interglacial. Clim. Past 7, 381–396.

Sachs, J.P., Schneider, R.R., Eglinton, T.I., Freeman, K.H., Ganssen, G., McManus, J.F., Oppo, D.W., 2000. Alkenones as paleoceanographic proxies. Geochem. Geophys. Geosyst. 1, 1035.

Schmidt, G.A., Annan, J.D., Bartlein, P.J., Cook, B.I., Guilyardi, E., Hargreaves, J.C., Harrison, S.P., Kageyama, M., LeGrande, A.N., Konecky, B., Lovejoy, S., Mann, M.E., Masson-Delmotte, V., Risi, C., Thompson, D., Timmermann, A., Tremblay, L.B., Yiou, P., 2014. Using palaeo-climate comparisons to constrain future projections in CMIP5. Clim. Past 10, 221–250.

Schurgers, G., Mikolajewicz, U., Gröger, M., Maier-Reimer, E., Vizcaino, M., Winguth, A., 2007. The effect of land surface changes on Eemian climate. Clim. Dyn. 29, 357–373.

Skinner, L.C., Shackleton, N.J., 2005. An Atlantic lead over Pacific deep-water change across Termination I: implications for the application of the marine isotope stage stratigraphy. Quaternary Science Reviews 24, 571–580.

Sime, L.C., Wolff, E.W., Oliver, K.I.C., Tindall, J.C., 2009. Evidence for warmer interglacials. Nature 462, 342–345.

Simstich, J., Sarnthein, M., Erlenkeuser, H., 2003. Paired δ^{18}O signals of Neogloboquadrina pachyderma (s) and Turborotalita quinqueloba show thermal

stratification structure in Nordic Seas. Mar. Micropaleontol. 48, 107–125 doi:110.1016/S0377-8398(1002)00165-00162.
Spahni, R., Chappellaz, J., Stocker, T.F., Loulergue, L., Hausammann, G., Kawamura, K., Fluckiger, J., Schwander, J., Raynaud, D., Masson-Delmotte, V., Jouzel, J., 2005. Atmospheric methane and nitrous oxide of the late Pleistocene from Antarctic ice cores. Science 310, 1317–1321.
Stenni, B., Selmo, E., Masson-Delmotte, V., Oerter, H., Meyer, H., Röthlisberger, R., Jouzel, J., Cattani, O., Falourd, S., Fischer, H., Hoffmann, G., Lacumin, P., Johnsen, S.J., Minster, B., 2010. The deuterium excess records of EPICA Dome C and Dronning Maud Land ice cores (East Antarctica). Quat. Sci. Rev. 29, 146–159.
Stocker, T.F., Johnsen, S.J., 2003. A minimum thermodynamic model for the bipolar seesaw. Paleoceanography 18, 1087.
Stone, E.J., Lunt, D.J., Annan, J.D., Hargreaves, J.C., 2013. Quantification of the Greenland ice sheet contribution to Last Interglacial sea level rise. Clim. Past 9, 621–639.
Telford, R.J., Li, C., Kucera, M., 2012. Mismatch between the depth habitat of planktonic foraminifera and the calibration depth of SST transfer functions may bias reconstructions. Clim. Past 8, 4075–4103.
Thompson, G., Curran, H.A., Wilson, M.A., White, B., 2011. Sea level oscillations during the last interglacial highstand recorded by Bahamas corals. Nat. Geosci. http://dx.doi.org/10.1038/ngeo1253.
Tolderlund, D.S., Bé, A.W.H., 1971. Seasonal distribution of planktonic foraminifera in the western North Atlantic. Micropaleontology 17, 297–329.
Turney, C.S.M., Jones, R.T., 2010. Does the Agulhas Current amplify global temperatures during super-interglacials? J. Quat. Sci. 25 (6), 839–843.
Van Nieuwenhove, N., Bauch, H.A., Eynaud, F., Kandiano, E., Cortijo, E., Turon, J.-L., 2011. Evidence for delayed poleward expansion of North Atlantic surface waters during the last interglacial (MIS 5e). Quat. Sci. Rev. 30, 934–946 doi:910.1016/j.quascirev.2011.1001.1013.
Veres, D., Bazin, L., Landais, A., Toyé Mahamadou Kele, H., Lemieux-Dudon, B., Parrenin, F., Martinerie, P., Blayo, E., Blunier, T., Capron, E., Chappellaz, J., Rasmussen, S.O., Severi, M., Svensson, A., Vinther, B., Wolff, E.W., 2013. The Antarctic ice core chronology (AICC2012): an optimized multi-parameter and multi-site dating approach for the last 120 thousand years. Clim. Past 9, 1733–1748 doi:1710.5194/cp-1739-1733-2013.
Villanueva, J., Grimalt, J.O., Cortijo, E., Vidal, L., Labeyrie, L., 1998. Assessment of sea surface temperature variations in the central North Atlantic using the alkenone unsaturation index (U^{k*}_{37}). Geochim. Cosmochim. Acta 62, 2421–2427.
Vinther, B.M., Buchardt, S.L., Clausen, H.B., Dahl-Jensen, D., Johnsen, S.J., Fisher, D.A., Koerner, R.M., Raynaud, D., Lipenkov, V., Andersen, K.K., Blunier, T., Rasmussen, S.O., Steffensen, J.P., Svensson, A.M., 2009. Holocene thinning of the Greenland ice sheet. Nature 461, 385–388.
Waelbroeck, C., Frank, N., Jouzel, J., Parrenin, F., Masson-Delmotte, V., Genty, D., 2008. Transferring radiometric dating of the last interglacial sea level high stand to marine and ice core records. Earth Planet. Sci. Lett. 265, 183–194.
Waelbroeck, C., Skinner, L.C., Labeyrie, L., Duplessy, J.-C., Michel, E., Vazquez Riveiros, N., Gherardi, J.-M., Dewilde, F., 2011. The timing of deglacial circulation changes in the Atlantic. Paleoceanography 26, PA3213. http://dx.doi.org/10.1029/2010PA002007.
Zamelczyk, K., Rasmussen, T.L., Husum, K., Haflidason, H., de Vernal, A., Krogh Ravna, E., Hald, M., Hillaire-Marcel, C., 2012. Paleoceanographic changes and calcium carbonate dissolution in the central Fram Strait during the last 20 ka. Quat. Sci. Rev. 78, 405–416.